Self-propelled colloids: from single to collective behaviour
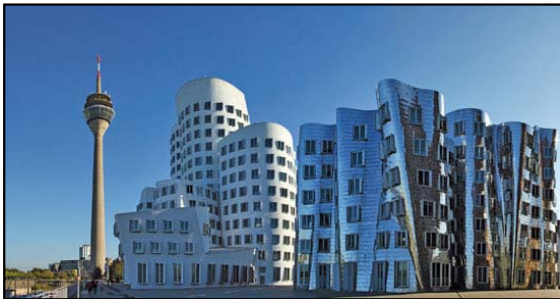
invited talk within the KITP program
"Active Matter: Cytoskeleton, Cells, Tissues and Flocks"
and within the Focused Workshop Group on "Self-Propelled Micro-Objects"
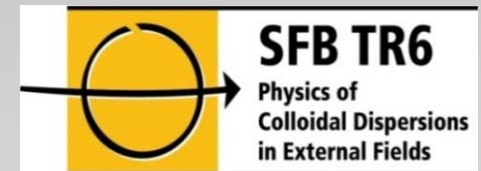
7.3.2014, Santa Barbara (USA)

by Hartmut Löwen,

A. Kaiser, A. Menzel, P. Cremer, H.H. Wensink,
R. Wittkowski, B. ten Hagen,
J. Bialké, T. Speck

Heinrich-Heine-Universität Düsseldorf

HEINRICH HEINE
UNIVERSITÄT DÜSSELDORF

SFB TR6
Physics of
Colloidal Dispersions
in External Fields

erc

penguins !

Zitterbart DP, Wienecke B, Butler JP, Fabry B (2011) Coordinated Movements Prevent Jamming in an Emperor Penguin Huddle. PLoS ONE 6(6): e20260.

I) Introduction

"active" (self-propelled) "particles" occur

in many different situations

- dissipation of energy

- intrinsically in nonequilibrium

- different from "passive" particles driven by external fields

goal of the talk: discuss simple models for (single and)

collective properties of active particles

From „passive" to „active" „particles"

Photo: Tero Pajukallio

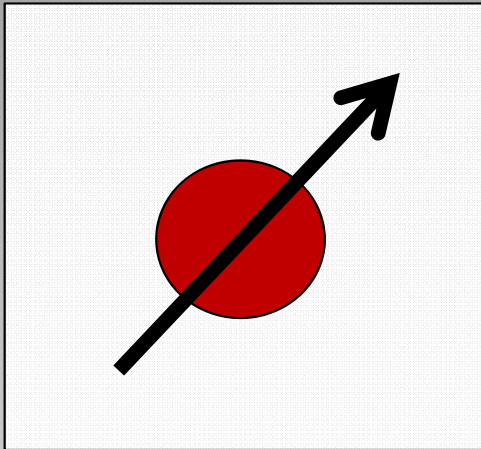http://www.geolinde.musin.de/europa/module/forest13_b.jpg

http://www.gartenteiche.de/files/2011/03/karpfenlaus_fischschwarm.jpg

passive   active

From „passive" to „active" particles
in the microworld (soft matter)

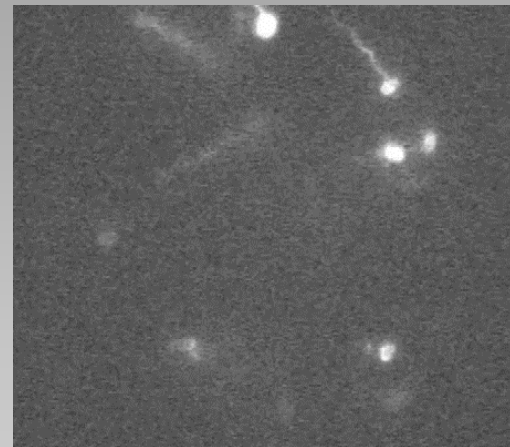**inert colloidal particle in an external field**

SFB TR6

Colloidal Dispersions in External Fields

(2002-2013)

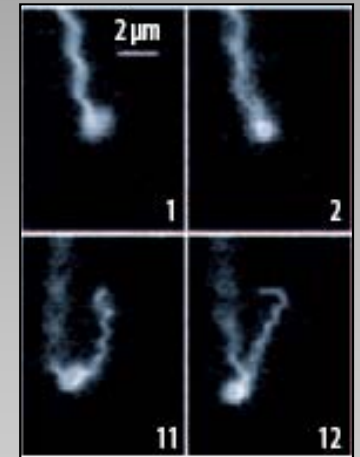http://www.youtube.com/watch?v=IEdb3wTMSBo

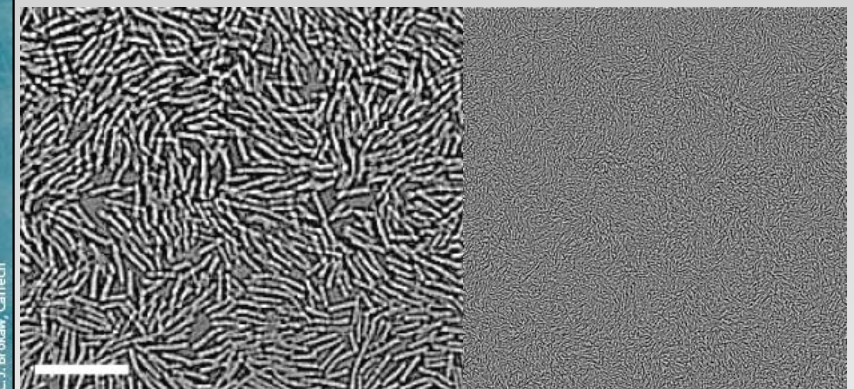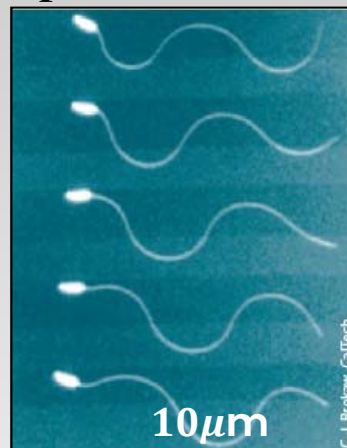**self-propelled „particles" with an internal motor**

- bacteria (E. coli)

http://www.rowland.harvard.edu/labs/bacteria/movies/showmovie.php?mov=fluo_semi-coil

- sperm

$10\mu m$

- bacillus subtilis
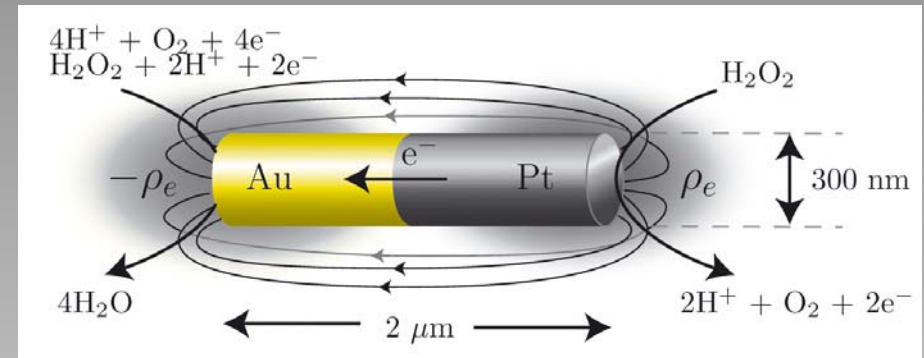
COLLOIDAL MICROSWIMMERS

catalytically driven colloidal Janus particles

W. F. Paxton et al, JACS **128**, 14881 (2006)

A. Erbe, M. Zientara, L. Baraban, C. Kreidler,
and P. Leiderer, J. Phys. Condens. Matter **20**, 404215 (2008)

G. Mino et al, PRL **106**, 048102 (2011)

I. Theurkauff, L. Bocquet et al, PRL **108**, 268303 (2012)

Thermally/diffusionally driven colloidal Janus particles

G. Volpe, I. Buttinoni, D. Vogt, H. Kümmerer, and C. Bechinger, Soft Matter **7**, 8810 (2011)

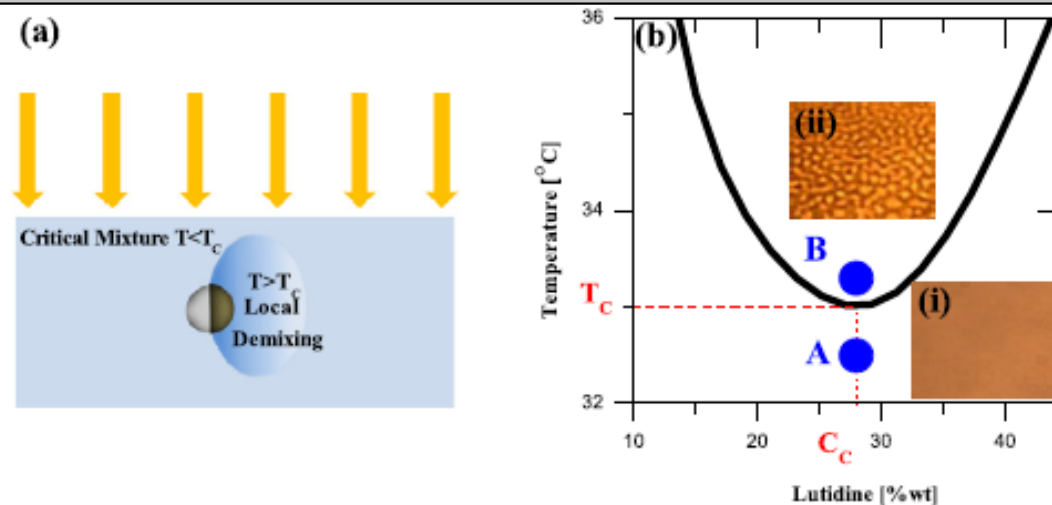**Figure 1.** Active Brownian micro-swimmers in a critical binary mixture. (a) Schematic explaining the self-propulsion mechanism: a Janus particle is illuminated and the cap is heated above T_c inducing a local demixing that eventually propels the particle. (b) A schematic phase diagram for water–2,6-lutidine. The insets are bright-field microscopy pictures of the mixed (i) and the demixed (ii) phase at the critical concentration.

Model: **Brownian dynamics of self-propelled rods**
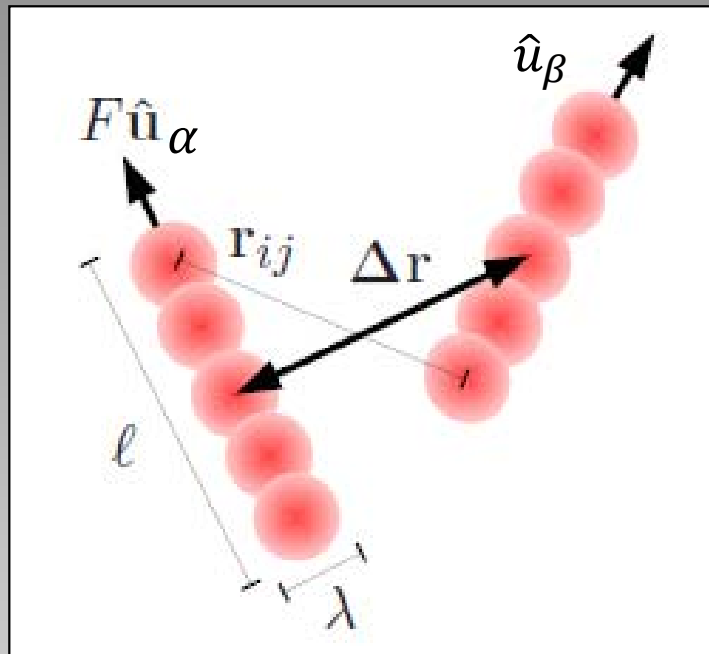
Yukawa segment interaction

$$U_{\alpha\beta} = \frac{U_0}{n^2} \sum_{i=1}^{n} \sum_{j=1}^{n} \frac{\exp[-(r_{ij}^{\alpha\beta}/\lambda)]}{r_{ij}^{\alpha\beta}}$$

$$r_{ij}^{\alpha\beta} = |\Delta\mathbf{r}_{\alpha\beta} + (l_i \hat{\mathbf{u}}_\alpha - l_j \hat{\mathbf{u}}_\beta)|$$

aspect ratio $a = \ell/\lambda$

n: number of segments

λ: screening length

Completely overdamped equations of motion

$$\mathbf{f}_T \cdot \partial_t \mathbf{r}_\alpha = -\nabla_{\mathbf{r}_\alpha} U + \boxed{F\hat{\mathbf{u}}_\alpha}$$

$$\mathbf{f}_R \cdot \partial_t \hat{\mathbf{u}}_\alpha = -\nabla_{\hat{\mathbf{u}}_\alpha} U.$$

internal drive

$$U = (1/2) \sum_{\beta,\alpha:\beta\neq\alpha} U_{\alpha\beta}$$

total potential energy

$$\mathbf{f}_T = f_0 \left[f_\| \hat{\mathbf{u}}_\alpha \hat{\mathbf{u}}_\alpha + f_\perp (\mathbf{I} - \hat{\mathbf{u}}_\alpha \hat{\mathbf{u}}_\alpha) \right]$$

$$\mathbf{f}_R = f_0 f_R \mathbf{I},$$

friction tensors for translation and rotation

Stokesian friction coefficient f_0

$$\frac{2\pi}{f_\|} = \ln a - 0.207 + 0.980 a^{-1} - 0.133 a^{-2}$$

$$\frac{4\pi}{f_\perp} = \ln a + 0.839 + 0.185 a^{-1} + 0.233 a^{-2}$$

$$\frac{\pi a^2}{3 f_R} = \ln a - 0.662 + 0.917 a^{-1} - 0.050 a^{-2}$$

explicit expressions for hard cylinders

(Tirado et al, JCP **81**, 2047 (1984))

- no hydrodynamic interactions

- no noise (zero temperature T=0), but noise can be included

- two spatial dimensions

length unit λ

time unit $\tau_0 = \lambda f_o / F$

energy unit $F\lambda$

remaining parameters of the model

$$\tilde{U}_0 = \frac{U_0}{F\lambda} = 250$$

$a = l/\lambda$ (aspect ratio)

$$\phi = \frac{N}{A}\left[\lambda(\ell - \lambda) + \frac{\pi\lambda^2}{4}\right]$$ effective volume fraction

Single particle limit

trivial linear trajectory along orientation û

û fixed

$$\vec{R}(t) = \vec{R}(0) + \frac{F}{f_0 f_{II}} \hat{u} t$$

Brownian noise for translation and rotation

➡ stochastic equations with known moments, see e.g.

B. ten Hagen, S. van Teeffelen, HL, J. Phys.: Condensed Matter **23**, 194119 (2011)

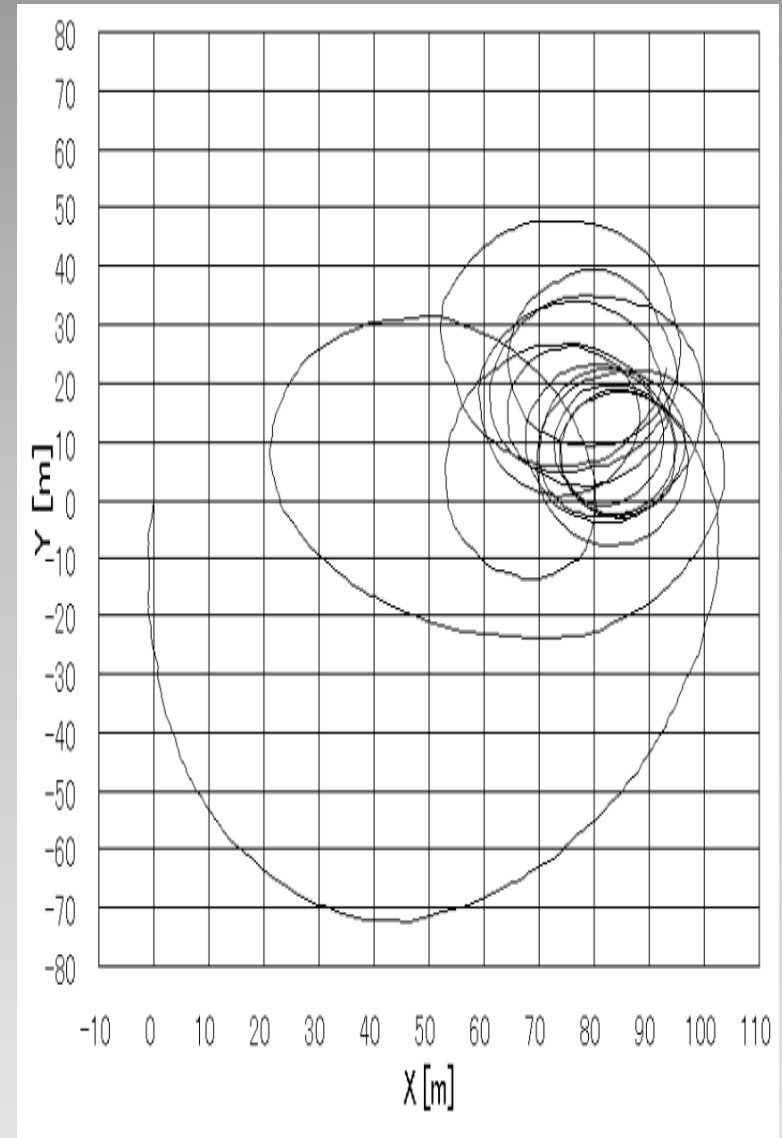also valid for circle swimmers (constant interval torque)

- PARENTHESIS -

interactions: ➡ **nontrivial collisions and many-body phenomena**

parenthesis: Brownian circle swimmers (1)
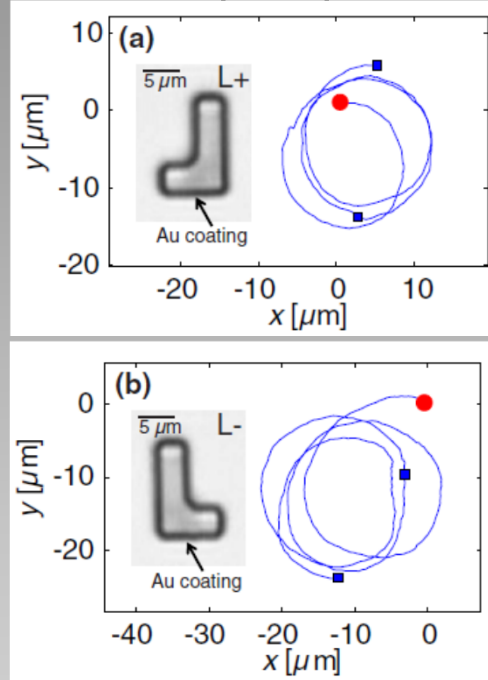
circling of human walkers

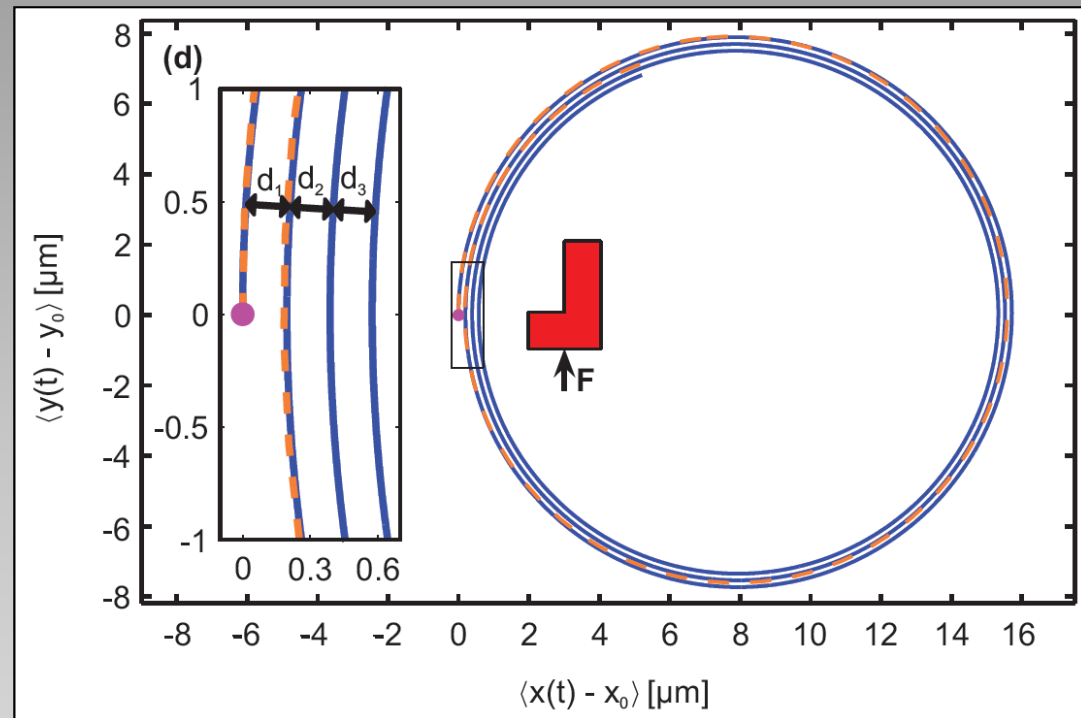- Trajectory of "Sample 5".

Obata *et al.*, *J. Korean Phys. Soc.* 2005

parenthesis: Brownian circle swimmers (2)

thermally driven colloidal Janus particles

chiral L-shaped particles

spira mirabilis for the noise-averaged trajectory

B. ten Hagen

Helical-like swimming in three dimensions: The Brownian spinning top

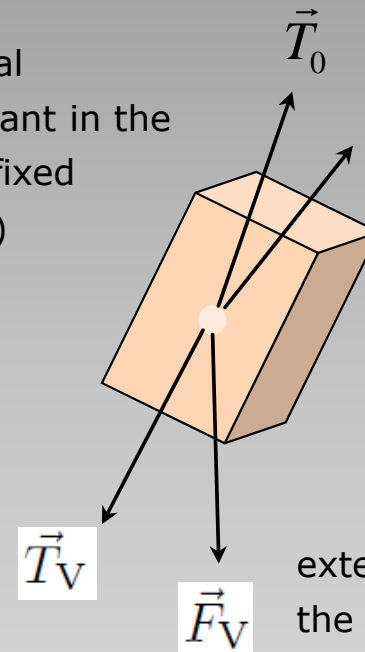**molecular dynamics**

ÜBER DIE THEORIE DES KREISELS, VOLUME 3

FELIX KLEIN, ARNOLD SOMMERFELD

1897–1910

self-propelled <u>biaxial</u> particle (in 3d)

internal (constant in the body-fixed frame)

$\vec{T}_0$

$\vec{F}_0$

R. Wittkowski

$$\vec{F}_V = -\vec{\nabla}_{\vec{r}} U$$

$$\vec{T}_V = -\vec{\nabla}_{\vec{\varpi}} U$$

$\vec{T}_V$

$\vec{F}_V$

external (constant in the lab-frame)

- complicated equations of motion (see de la Torre et al, Doi for passive particles)

- translation-rotation coupling for a chiral particle (Brenner et al)

Single particle limit

trivial linear trajectory along orientation û

û fixed

$$\vec{R}(t) = \vec{R}(0) + \frac{F}{f_0 f_{II}} \hat{u} t$$

Brownian noise for translation and rotation

➡ stochastic equations with known moments, see e.g.

B. ten Hagen, S. van Teeffelen, HL, J. Phys.: Condensed Matter **23**, 194119 (2011)
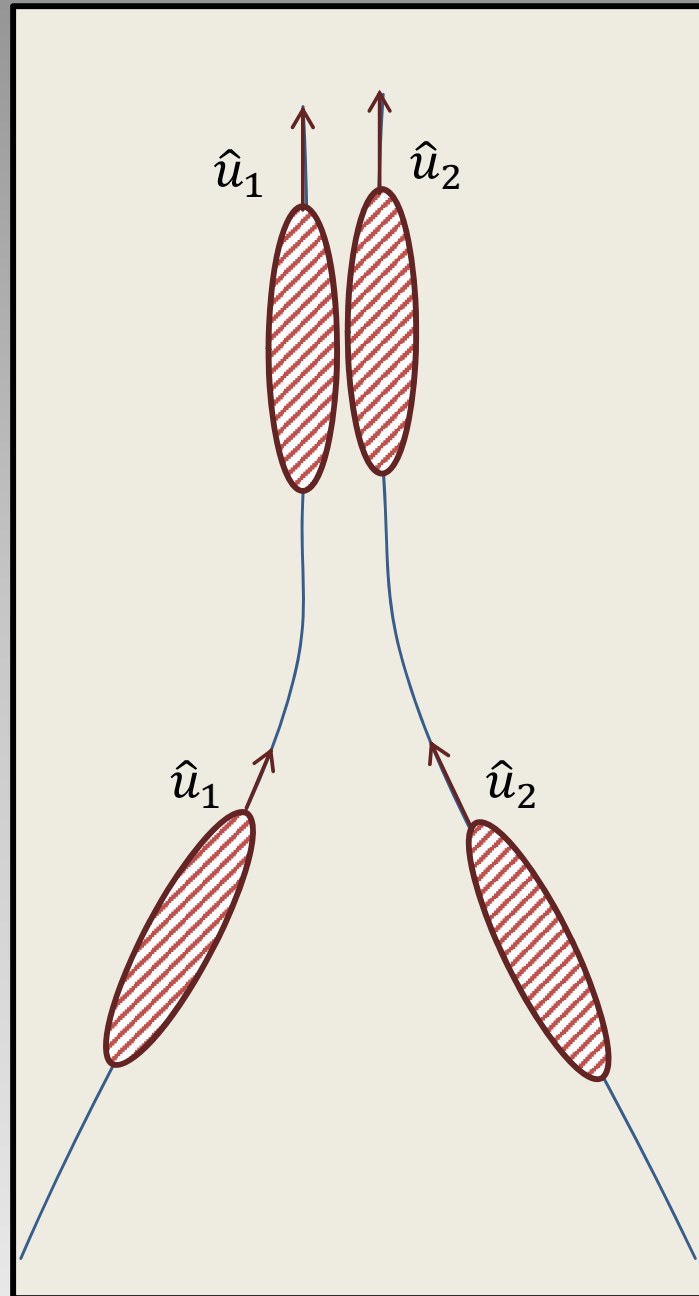
also valid for circle swimmers (constant interval torque)

interactions: ➡ **nontrivial collisions and many-body phenomena**

binary collisions

non-central
forces

non-elastic
collisions

$\hat{u}_1$ $\hat{u}_2$

$\hat{u}_1$ $\hat{u}_2$

tendency of

mutual alignment

$\longrightarrow$ swarming

(Viczek et al, I. Aranson)
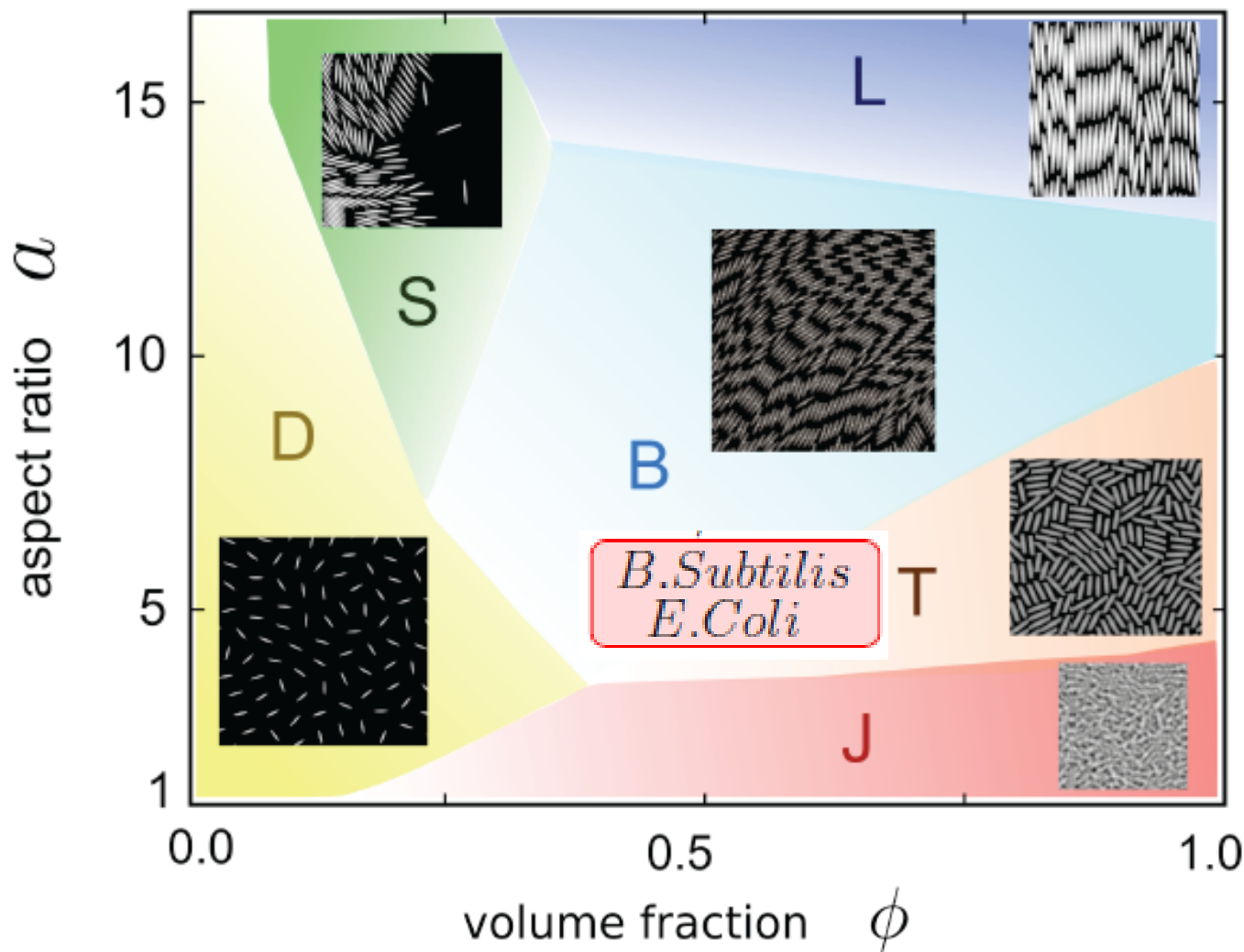
II) Meso-scale turbulence in living fluids

Fig. 1. (A) Schematic non-equilibrium phase diagram of the 2D SPR model and snapshots of six distinct phases from simluations: D-dilute state, J-jamming, S-swarming, B-bionematic phase, T-turbulence, L-laning. Our analysis focusses on the bionematic and turbulent regimes B/T

- no temperature,
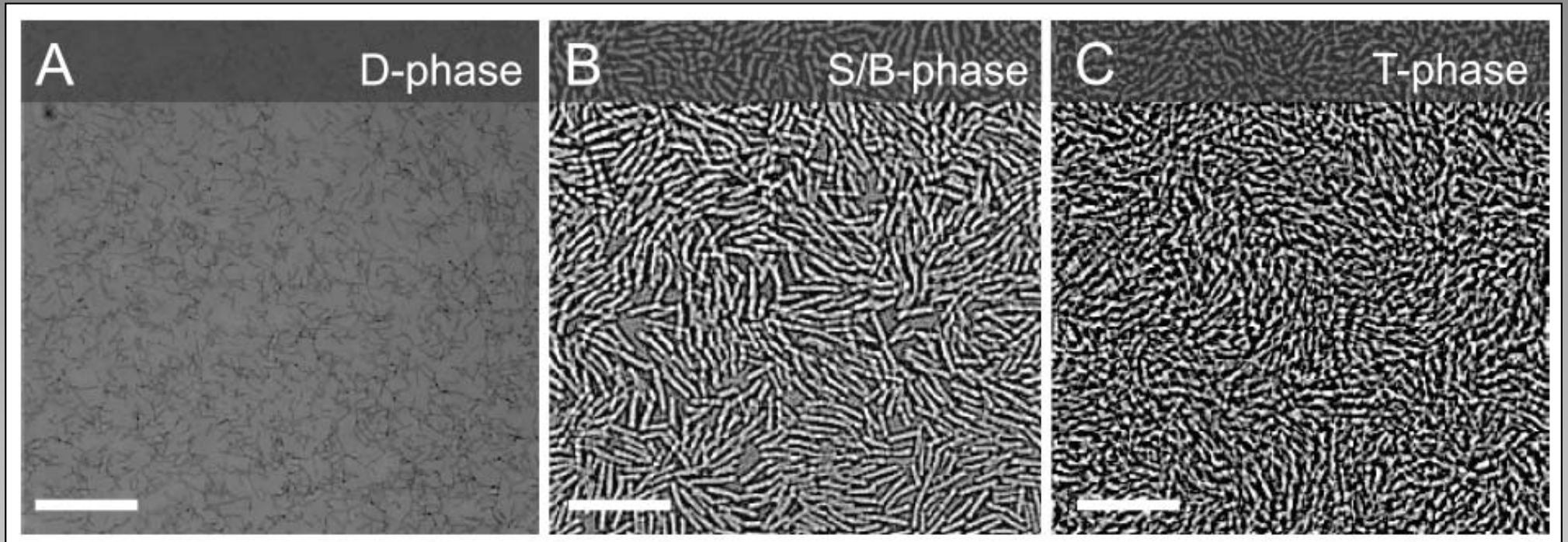- repulsive Yukawa segment interactions, swarming behaviour
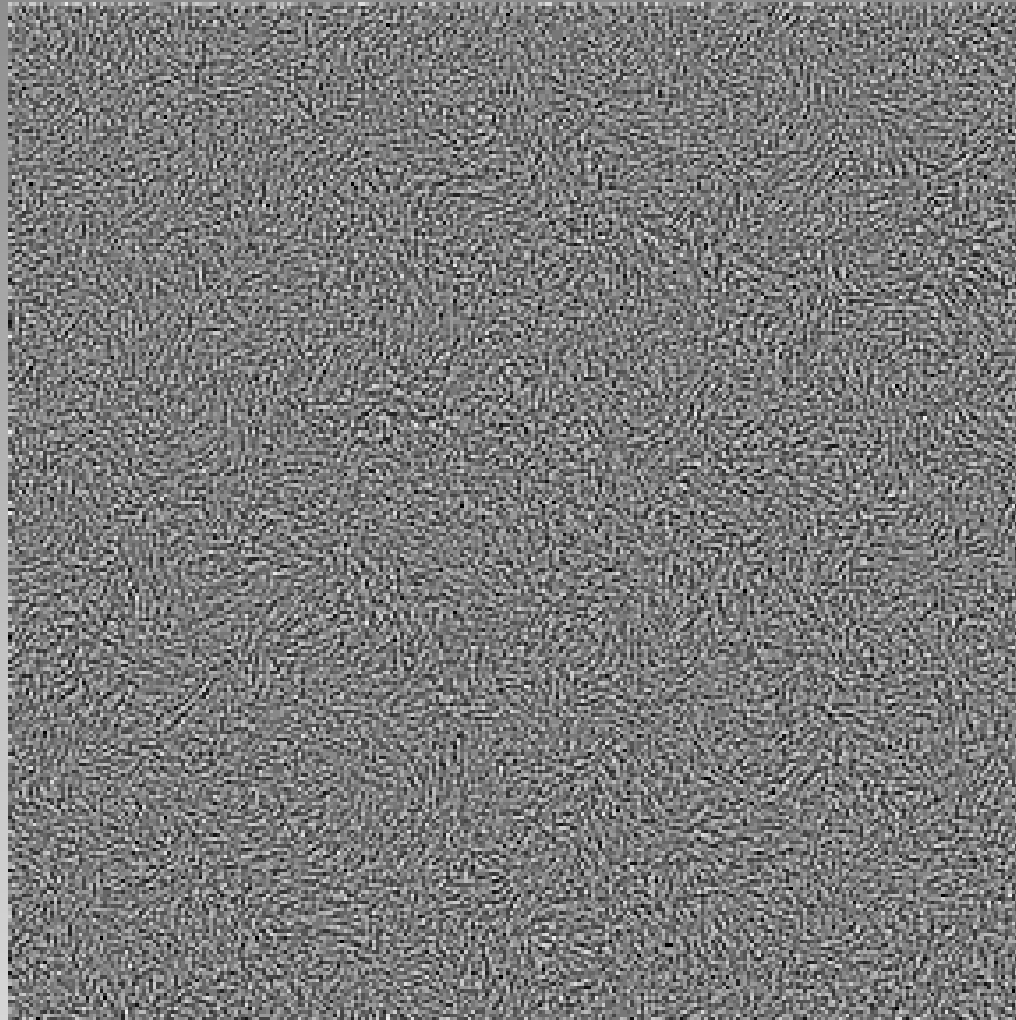
H. H. Wensink and HL

J. Phys.: Condensed Matter **24**, 460130 (2012)

H. H. Wensink et al,

PNAS **109**, 14308 (2012)

experiments on 2d-confined solutions (Drescher, Goldstein et al) of bacillus subtilis

turbulent phase in a quasi-2D homogeneous B. subtilis suspension (channel thickness approximately 5 µm).

Continuum model (generalization of Toner-Tu theory)

$$\nabla \cdot v = \partial_i v_i = 0, \qquad i = 1, \ldots, d,$$

incompressibility

$$(\partial_t + v \cdot \nabla)v = -\nabla p - (\alpha + \beta |v|^2)v + \nabla \cdot E,$$

Navier-Stokes equation

$$E_{ij} = \Gamma_0(\partial_i v_j + \partial_j v_i) - \Gamma_2 \triangle (\partial_i v_j + \partial_j v_i) + S q_{ij},$$

rate-of strain-tensor E

$$q_{ij} = v_i v_j - \frac{\delta_{ij}}{d}|v|^2$$

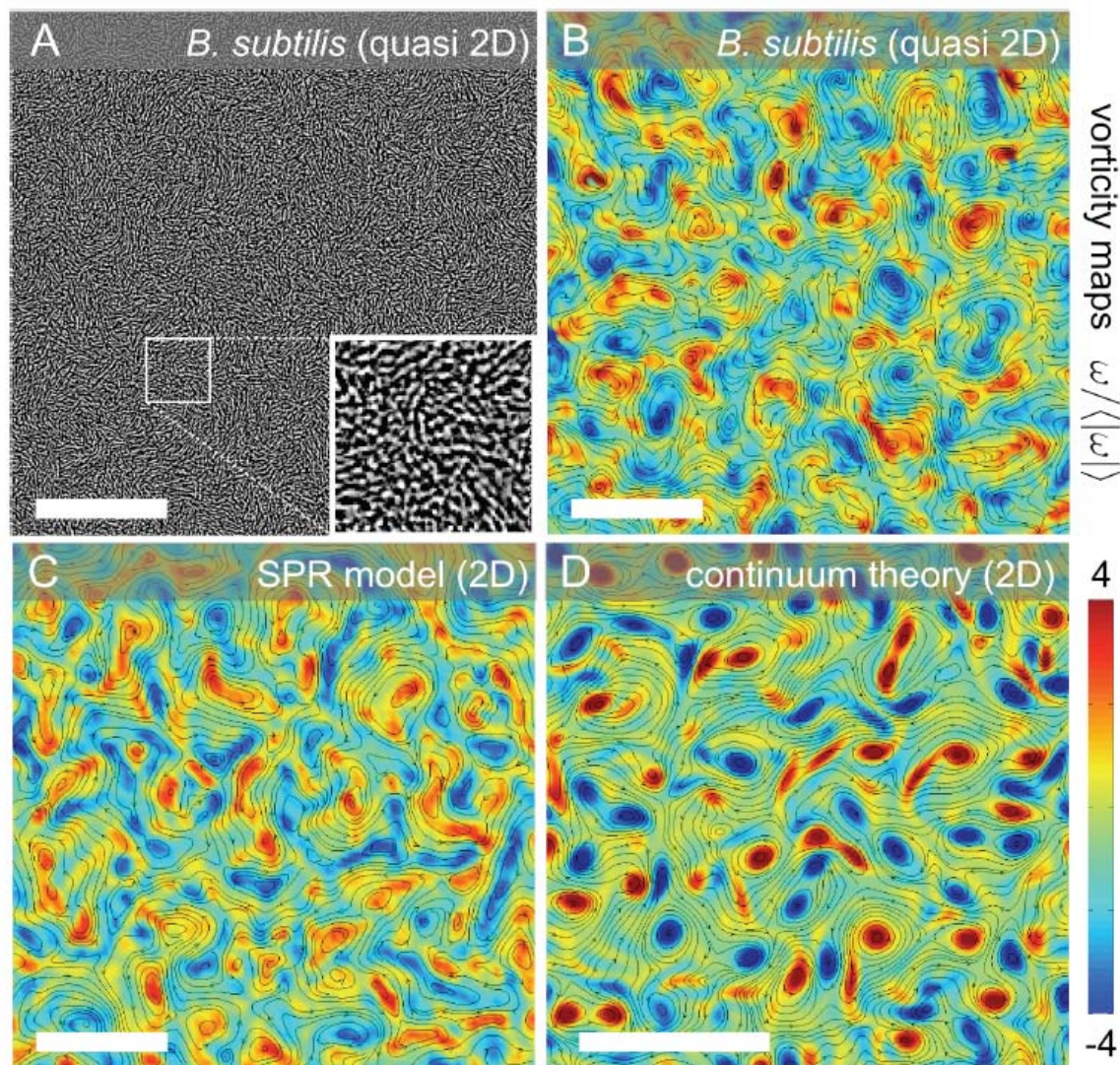see also: J. Dunkel, S. Heidenreich et al, PRL 110, 228102 (2013)

Fig. 2. Experimental snapshot (A) of a highly concentrated, homogeneous quasi-2D bacterial suspension (see also Movie S07 and Fig. S8). Flow streamlines $\boldsymbol{v}(t, \boldsymbol{r})$ and vorticity fields $\omega(t, \boldsymbol{r})$ in the turbulent regime, as obtained from (B) quasi-2D bacteria experiments, (C) simulations of the deterministic SPR model ($a = 5$, $\phi = 0.84$), and (D) continuum theory. The range of the simulation data in (D) was adapted to the experimental field of view ($217\ \mu\text{m} \times 217\ \mu\text{m}$) by matching the typical vortex size (scale bars $50\mu\text{m}$). Simulation parameters are summarized in the SI Text.
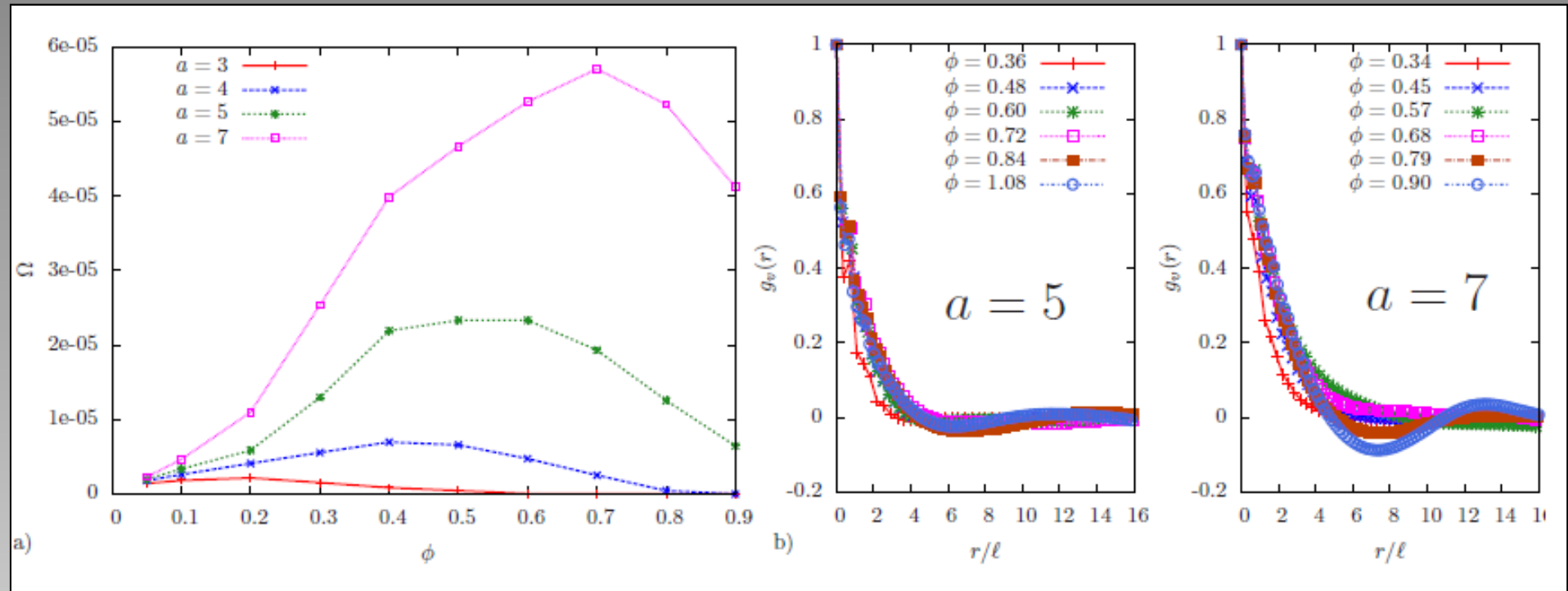
Figure 5. (a) Enstrophy Ω (in units τ_0^{-2}) versus filling fraction for a number of aspect ratios a in the turbulent regime. The maxima correspond to the densities where mixing due to vortical motion is the most efficient. (b) Spatial velocity autocorrelation function for a number of bulk volume fractions in the turbulent flow regime for two different aspect ratios a.

energy spectrum:

$$E(k) \sim k \int d\boldsymbol{r} \exp[-i\boldsymbol{k} \cdot \boldsymbol{r}] \langle \boldsymbol{v}(t,0) \cdot \boldsymbol{v}(t,\boldsymbol{r}) \rangle_t$$

Fourier transform of the VACF

Kolmogorov-Kraichnan scaling for 2d classical turbulence:

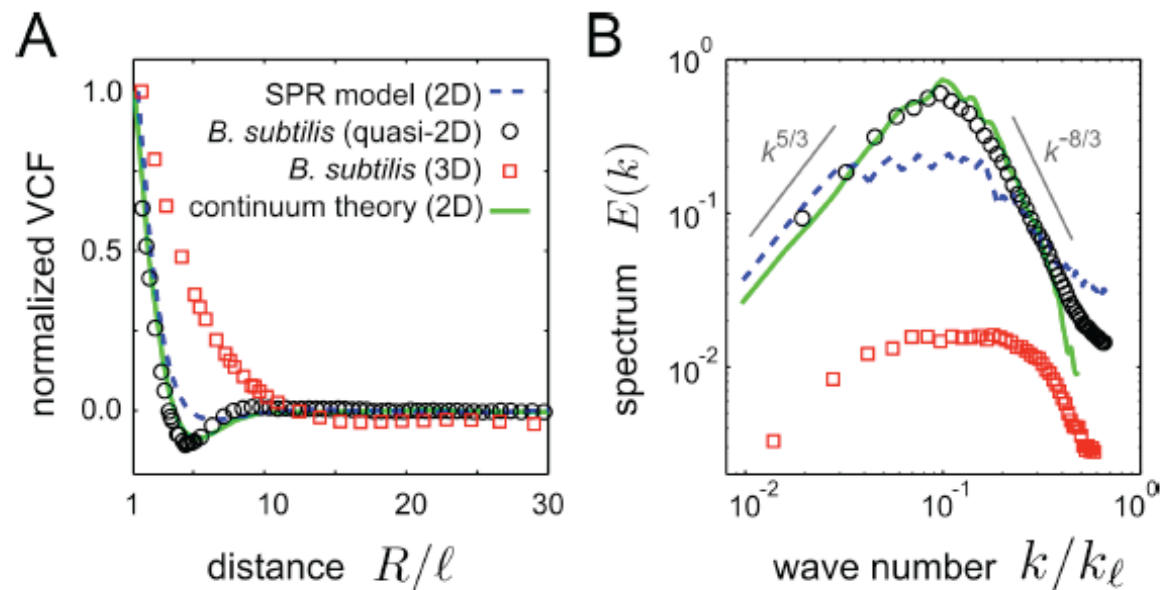$$E(k) \propto k^{-5/3}$$

(inertial regime)

Fig. 4. Equal-time velocity correlation functions (VCFs), normalized to unity at $R = \ell$, and flow spectra for the 2D SPR model ($a = 5$, $\phi = 0.84$), *B. subtilis* experiments, and 2D continuum theory based on the same data as in Fig. 3. (A) The minima of the VCFs reflect the characteristic vortex size R_v [47]. Data points present averages over all directions and time steps to maximize sample size. (B) For bulk turbulence (red squares) the 3D spectrum $E_3(k)$ is plotted ($k_\ell = 2\pi/\ell$), the other curves show 2D spectra $E_2(k)$. Spectra for the 2D continuum theory and quasi-2D experimental data are in good agreement; those of the 2D SPR model and the 3D bacterial data show similar asymptotic scaling but exhibit an intermediate plateau region (spectra multiplied by constants for better visibility and comparison).

- not consistent with Kolmogorov-Kraichnan scaling

    self-sustained turbulence!

- maximal swirl size

H. H. Wensink, J. Dunkel, S. Heidenreich,, K. Drescher, R. Goldstein, H. Löwen, J. M. Yeomans, *Meso-scale turbulence in living fluids*, PNAS **109**, 14308 (2012).

Summary

- At high density there is mesoscale turbulence in living or active fluids „bacterial turbulence"

- The energy spectrum does not follow Kolmogorov-Kraichnan scaling

What to do with bacterial turbulence?

length units in μm

118

28

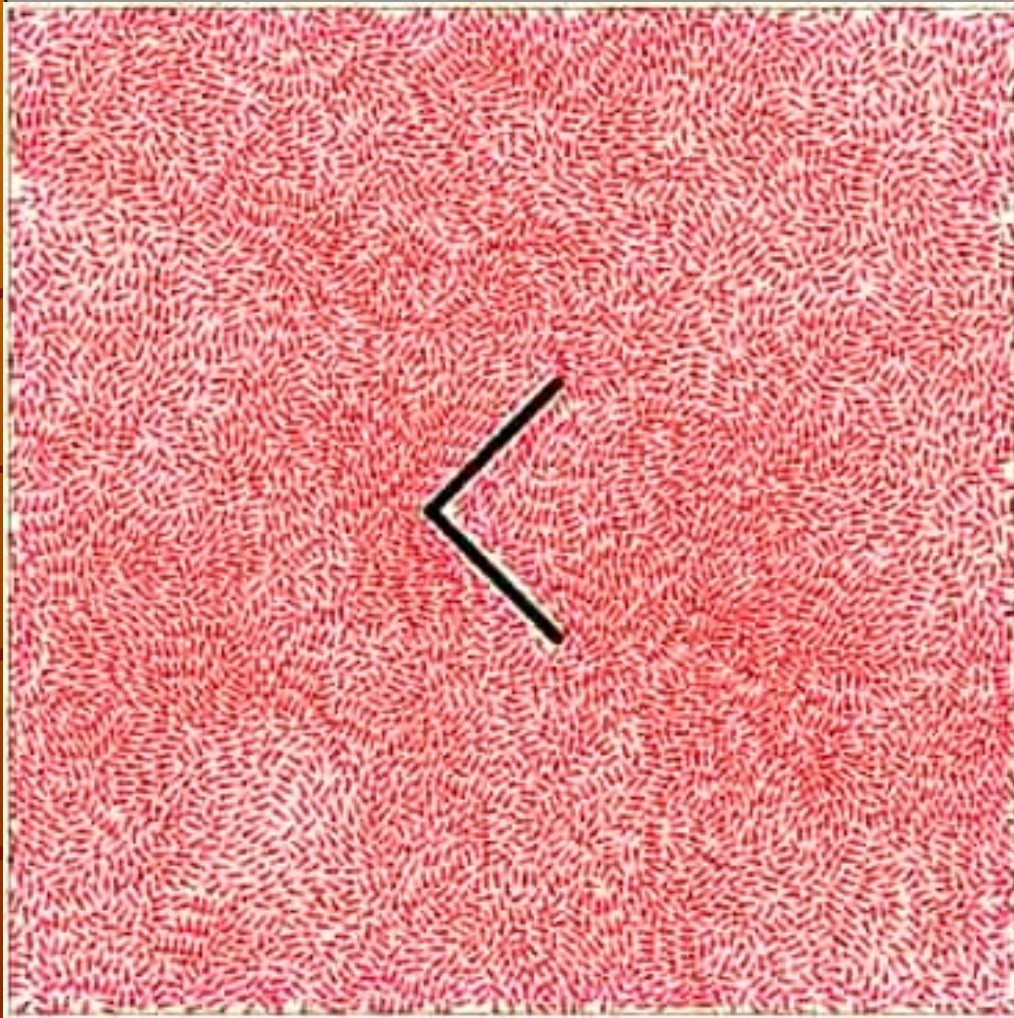186
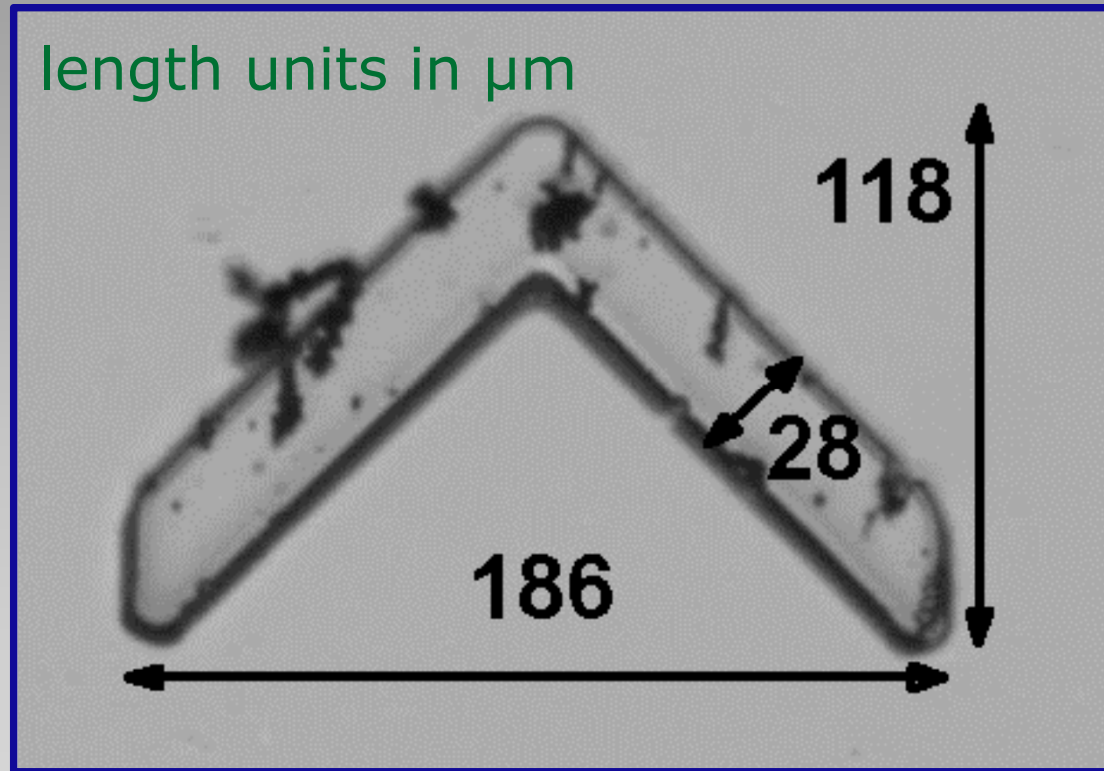
mesoscopic carrier, „bulldozer"

Andreas Kaiser
(Düsseldorf)
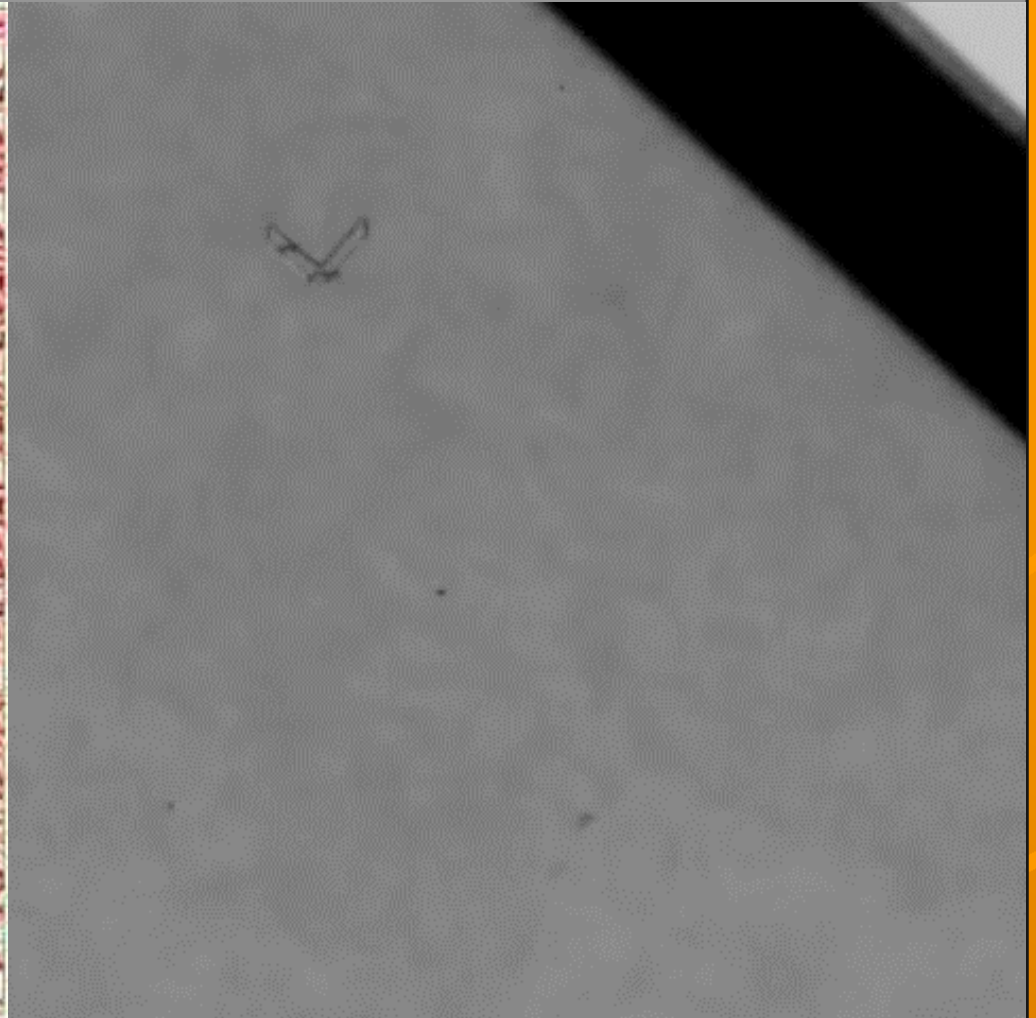

Borge ten Hagen
(Düsseldorf)

with I. Aranson, A.Peshkov (Argonne), A. Sokolov (Paris)
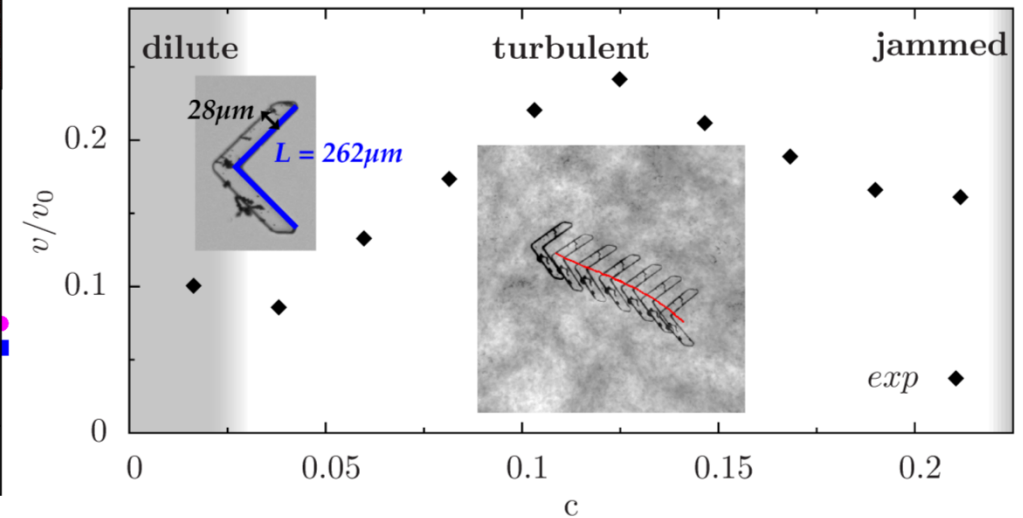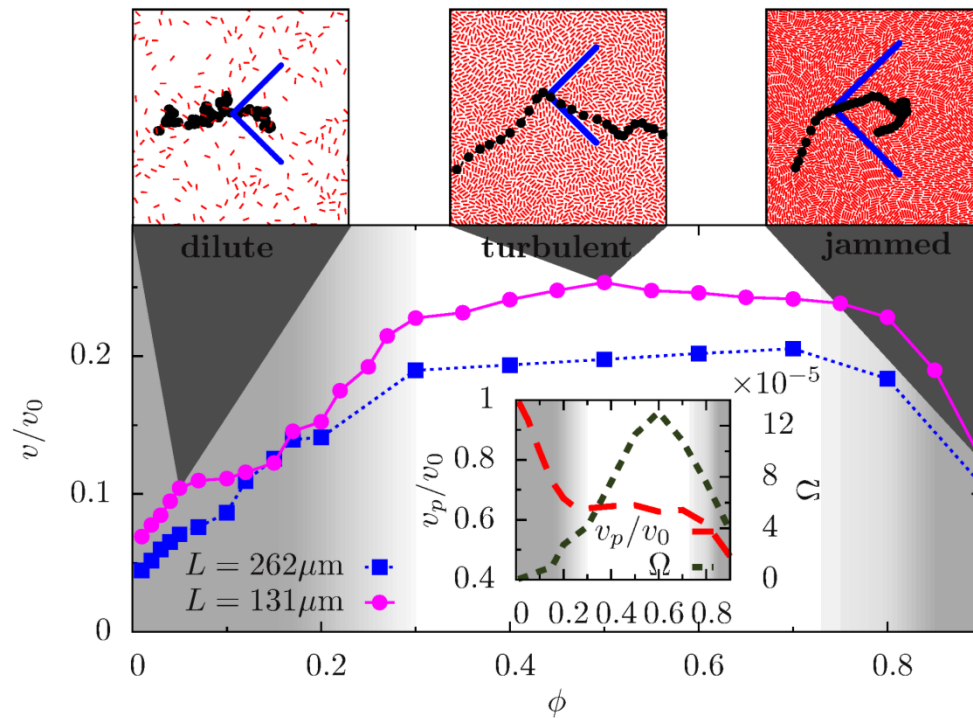
simulation   experiment

simulation   experiment

turbulence maximizes transport efficiency

idea: extract useful mechanical energy out of turbulence

transport mechanism

swirl depletion

simulation

experiment

$\phi = 0.2$

x/ℓ
-15 0 15

x/ℓ
-15 0 15

$c = 0.12$

y/ℓ

15

0

-15

$\phi = 0.7$

y/ℓ

15

0

-15

shielded area

unshielded area

R

0   0.5   1
enstrophy
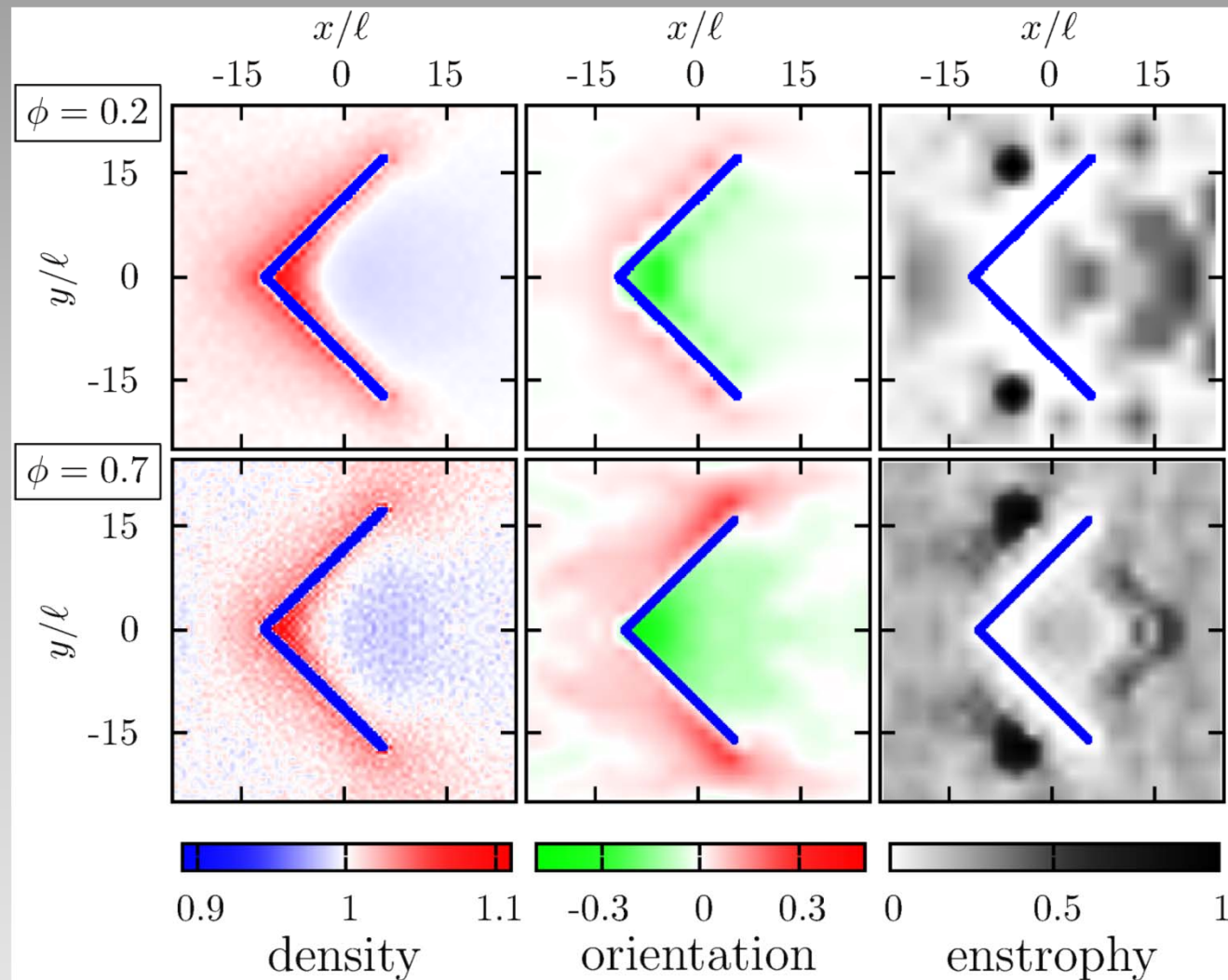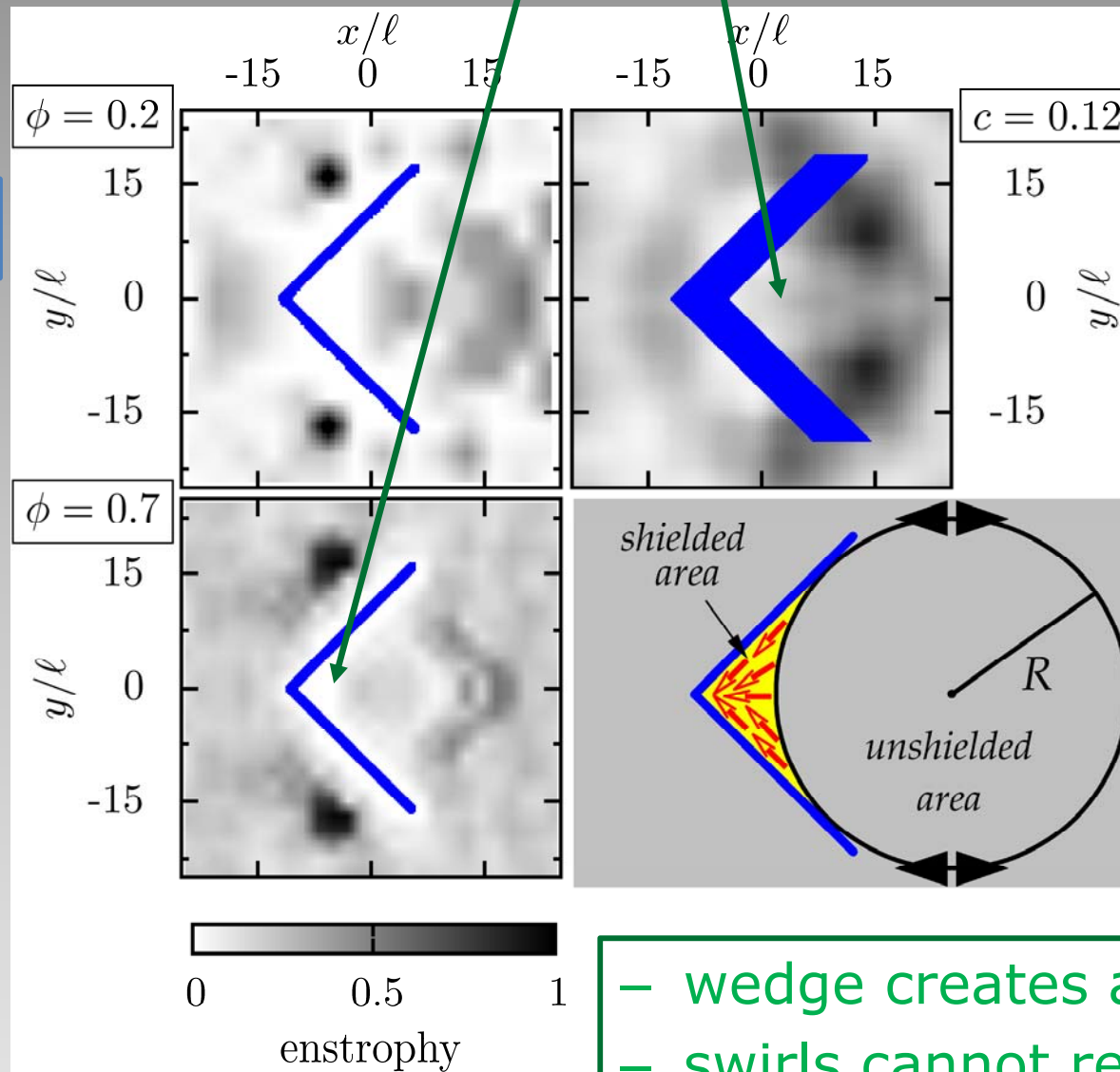
− wedge creates a shielded area
− swirls cannot reach cusp

How to clean the corners?
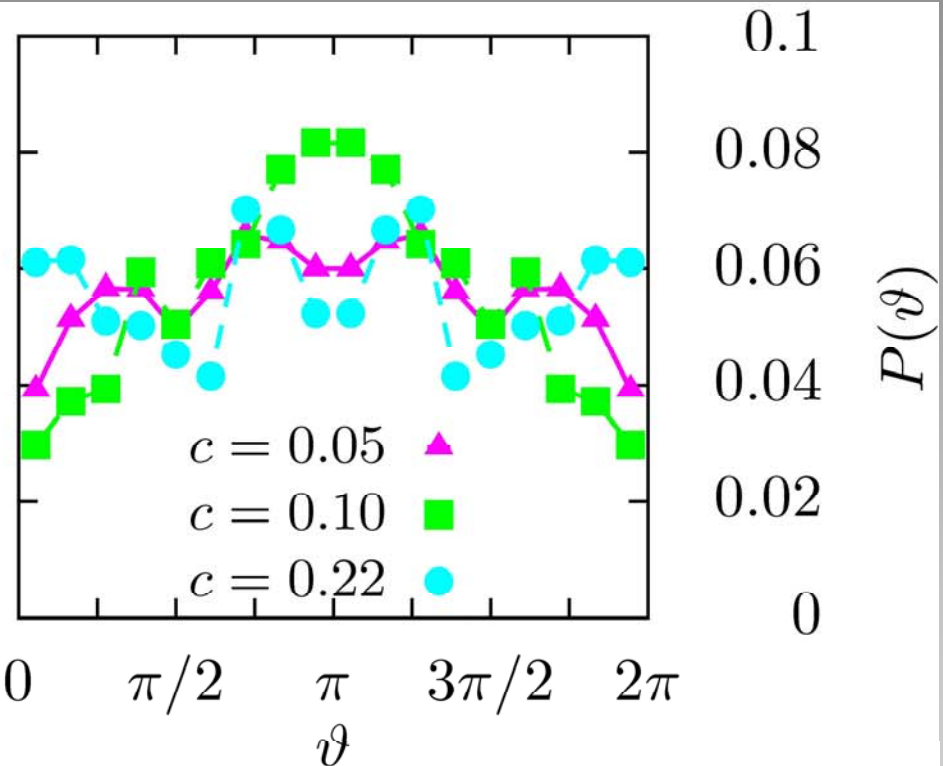
- low concentration: direction (almost) random
- intemediate concentration: directed along x-axis
- high concentration: occurrence of a double peak
  -> zig-zag motion

underlying reason for tilted carrier motion

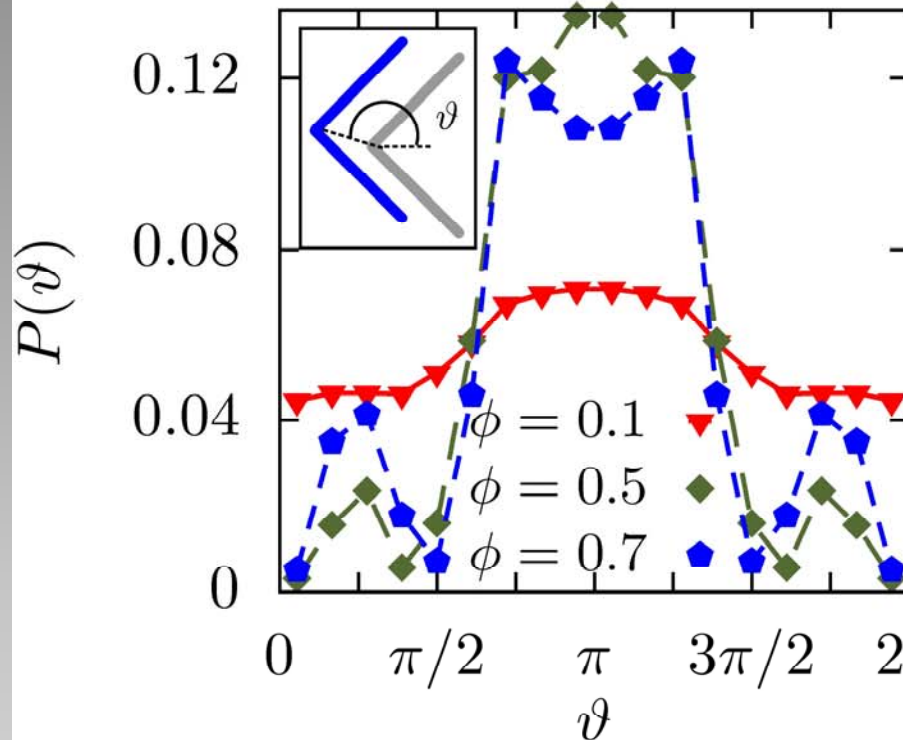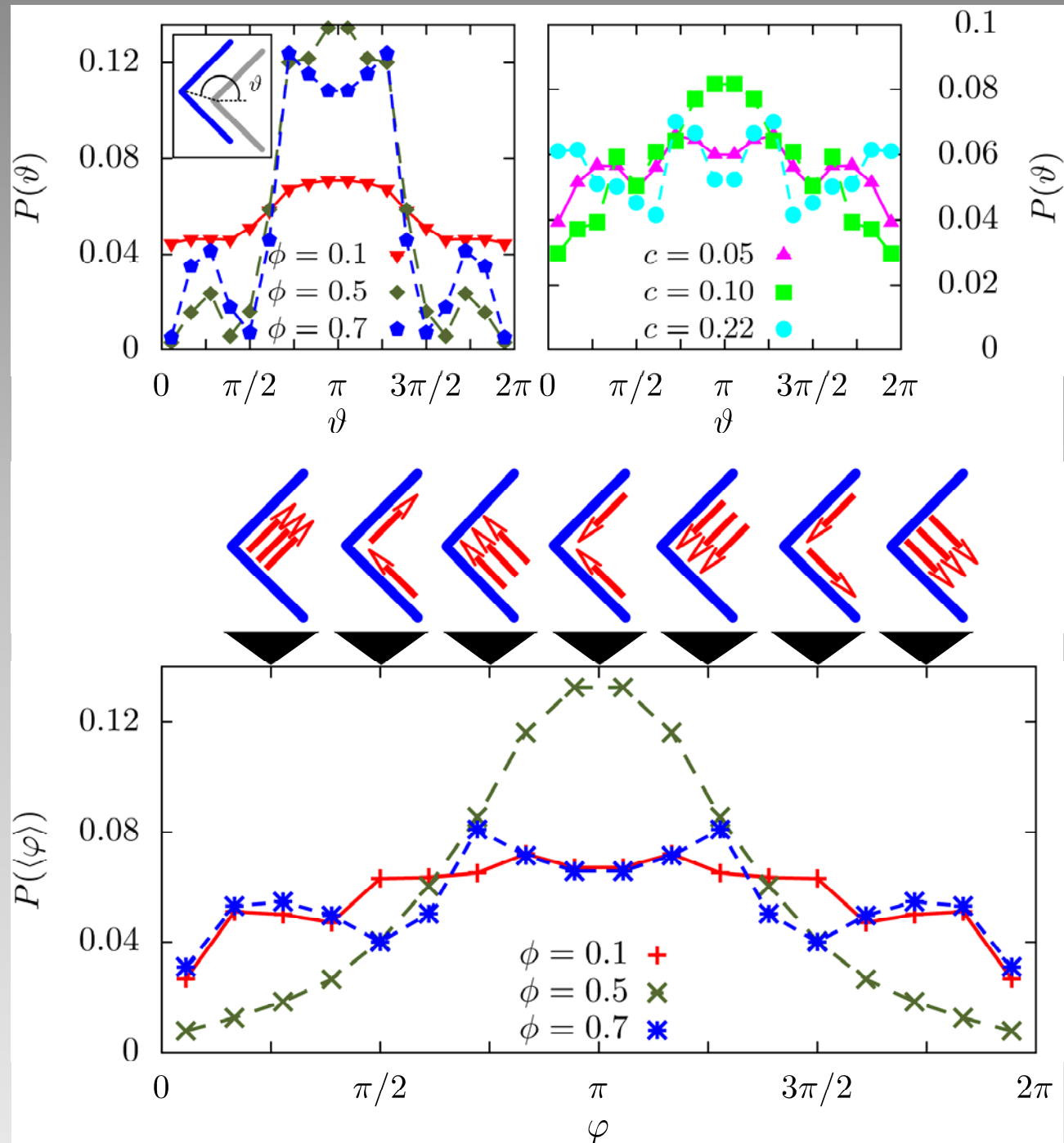# IV) Crystallization for active particles

Julian Bialké

Thomas Speck

spherical particles (one segment)

2d

plus noise

($\hat{=}$ finite temperature in equilibrium)

rotational noise decoupled (minimal model)

interaction coupling parameter

$$\Gamma = v_0 \sqrt{\rho} / k_B T$$

propulsion strength

$$f = \frac{F}{k_B T \sqrt{\rho}}$$

J. Bialké, T. Speck, HL, PRL **108**, 168301 (2012)

FIG. 1 (color online). Cooling (solid lines) and melting curves (dashed lines) for (a) the orientational order parameter ψ_6 and (b) the long-time dif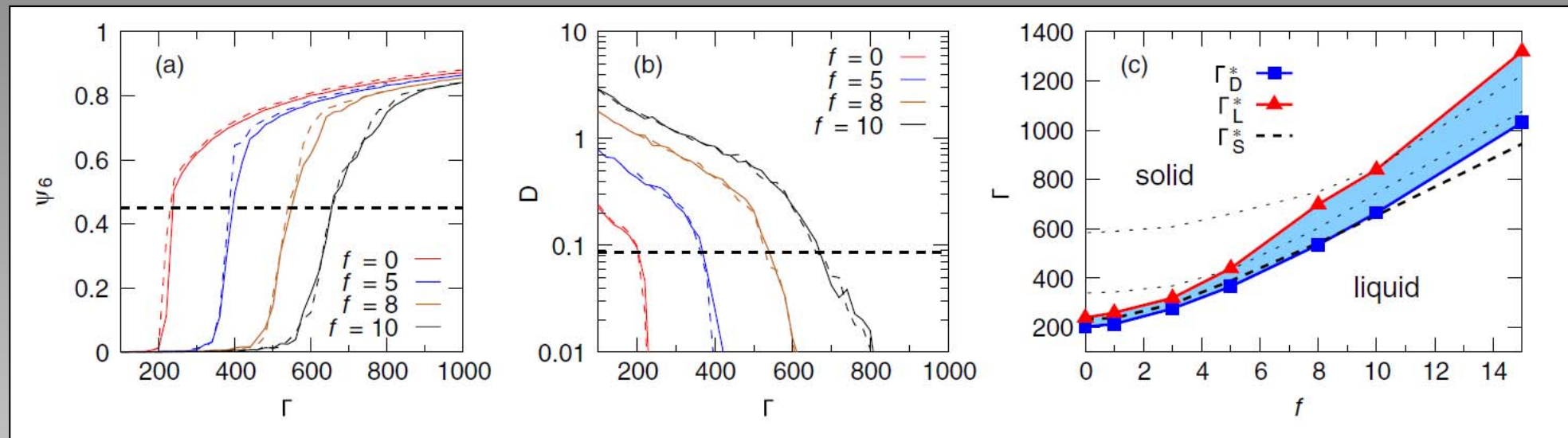fusion coefficient D vs the potential strength Γ for selected driving forces f. The crossings with the dashed horizontal lines define the position of the structural transition Γ_S^* ($\psi_6 = 0.45$) and the dynamical freezing Γ_D^* ($D = 0.086$), respectively. (c) Phase diagram in the f-Γ plane. The symbols mark the numerically estimated dynamical freezing line Γ_D^* and melting line Γ_L^* (see main text for definition). The thick dashed line indicates the structural transition Γ_S^*. Also plotted are the $\psi_6 = 0.67$ and $\psi_6 = 0.8$ "isostructure" lines along which ψ_6 is constant.

with drive: structural and dynamical diagnostics of freezing differ !

snapshot across
the freezing
transition
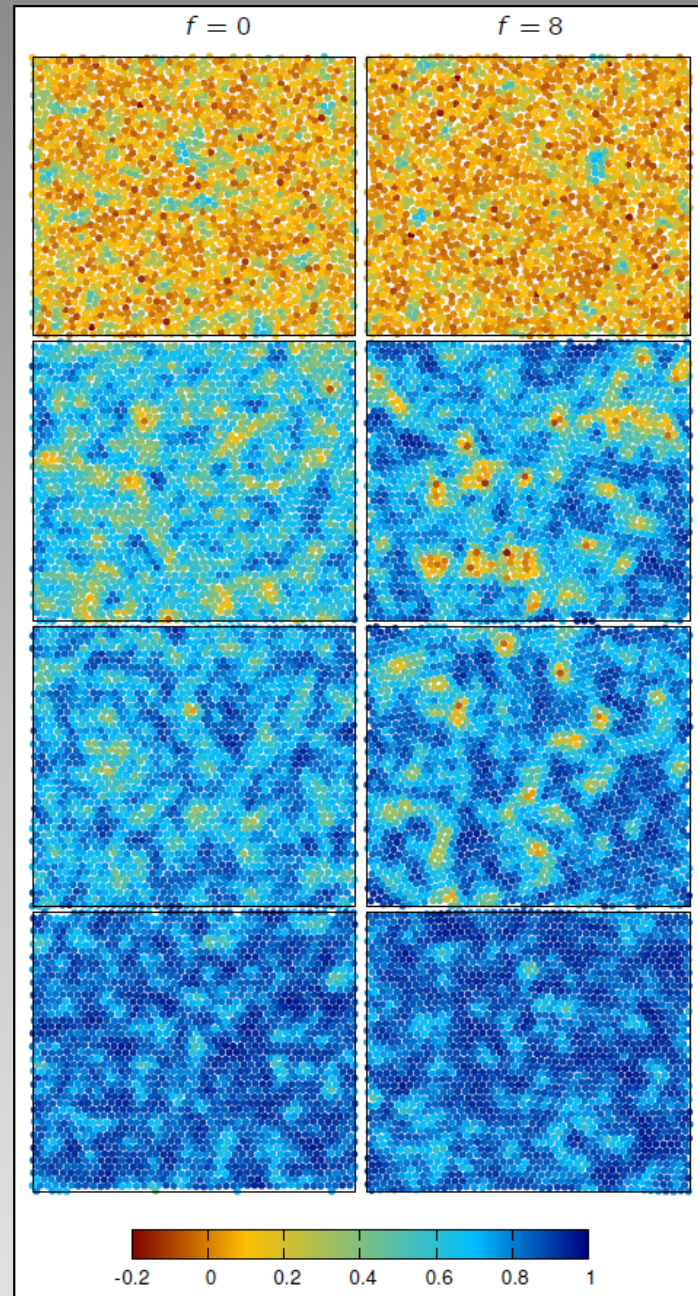
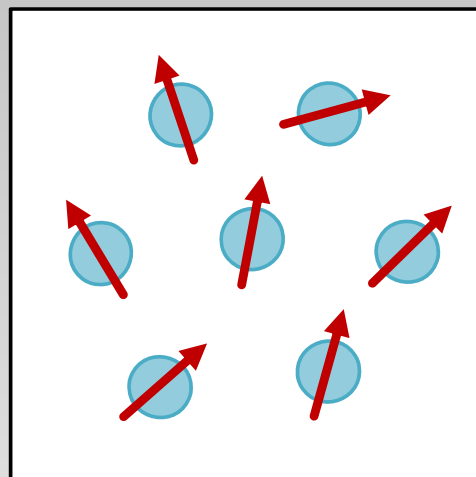„bubbles"

without propulsion | with self propulsion

Phase-Field-Crystal (PFC) plus Toner-Tu

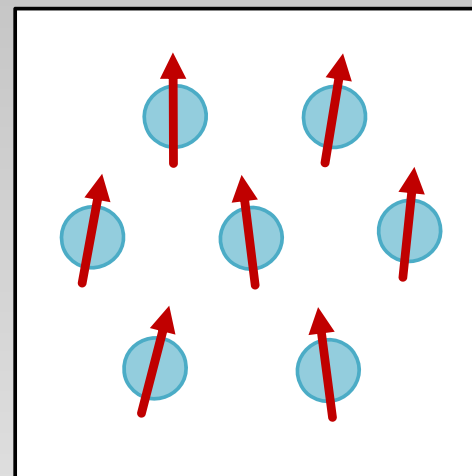Andreas Menzel

microscopic field-theoretical model for crystallization

⇨ **travelling and resting crystals**

no migration

direction of

migration

resting crystal

travelling crystal

cf: Gregoire, Chaté, Tu, Physica D **181**, 157 (2003)

$\psi_1(\vec{r}, t)$ density field $\vec{P}(\vec{r}, t)$ polarization field   as coupled order parameters

$$\partial_t \psi_1 = \nabla^2 \frac{\delta \mathcal{F}}{\delta \psi_1} - v_0 \nabla \cdot \mathbf{P},$$

PFC model   K. Elder et al, PRL **88**, 245701 (2002)

$$\partial_t \mathbf{P} = \nabla^2 \frac{\delta \mathcal{F}}{\delta \mathbf{P}} - D_r \frac{\delta \mathcal{F}}{\delta \mathbf{P}} - v_0 \nabla \psi_1$$

reduced Toner-Tu model   Toner, Tu, PRL **75**, 4326 (1995)

self-propagation speed

total functional $\mathcal{F} = \mathcal{F}_{pfc} + \mathcal{F}_{\mathbf{P}}$

with $$\mathcal{F}_{pfc} = \int d^2r \left\{ \frac{1}{2} \psi \left[\varepsilon + (1 + \nabla^2)^2 \right] \psi + \frac{1}{4} \psi^4 \right\}$$

and $$\mathcal{F}_{\mathbf{P}} = \int d^2r \left\{ \frac{1}{2} C_1 \mathbf{P}^2 + \frac{1}{4} C_4 (\mathbf{P}^2)^2 \right\}$$

either $c_1 > 0$ or $c_1 < 0$ and $c_4 > 0$

resting crystal

travelling crystal (hex)

travelling
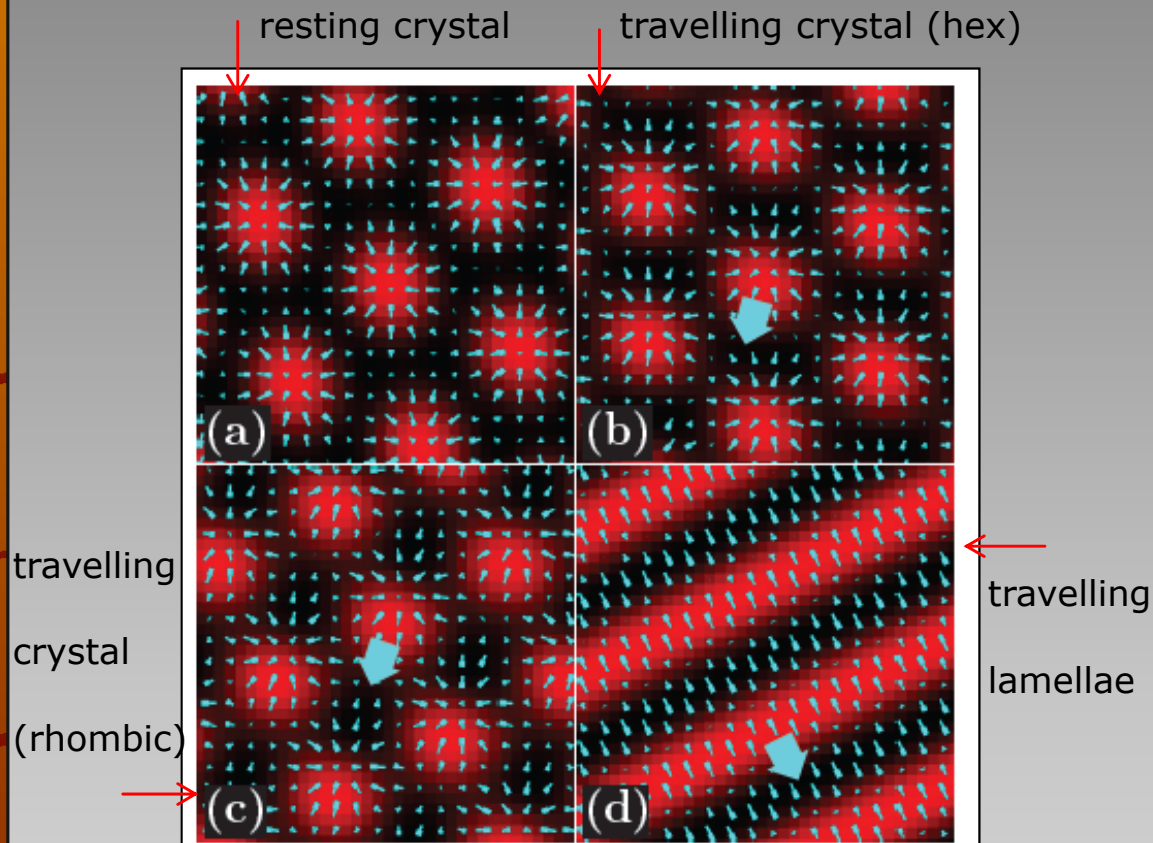
crystal

(rhombic)

travelling

lamellae

FIG. 2. Different phases observed when increasing the active drive v_0 at $(\bar{\psi}, \varepsilon, C_1, C_4) = (-0.4, -0.98, 0.2, 0)$: (a) resting hexagonal, $v_0 = 0.1$, (b) traveling hexagonal, $v_0 = 0.5$, (c) traveling quadratic, $v_0 = 1$, (d) traveling lamellar, $v_0 = 1.9$. The phases are depicted by plotting the density field ψ_1. Thin bright needles illustrate the polarization field $\mathbf{P}$ that points from the thick to the thin ends. In panels (b)–(d) the predominant direction of motion is indicated by the bright arrows. Only a fraction of the numerical calculation box is shown.
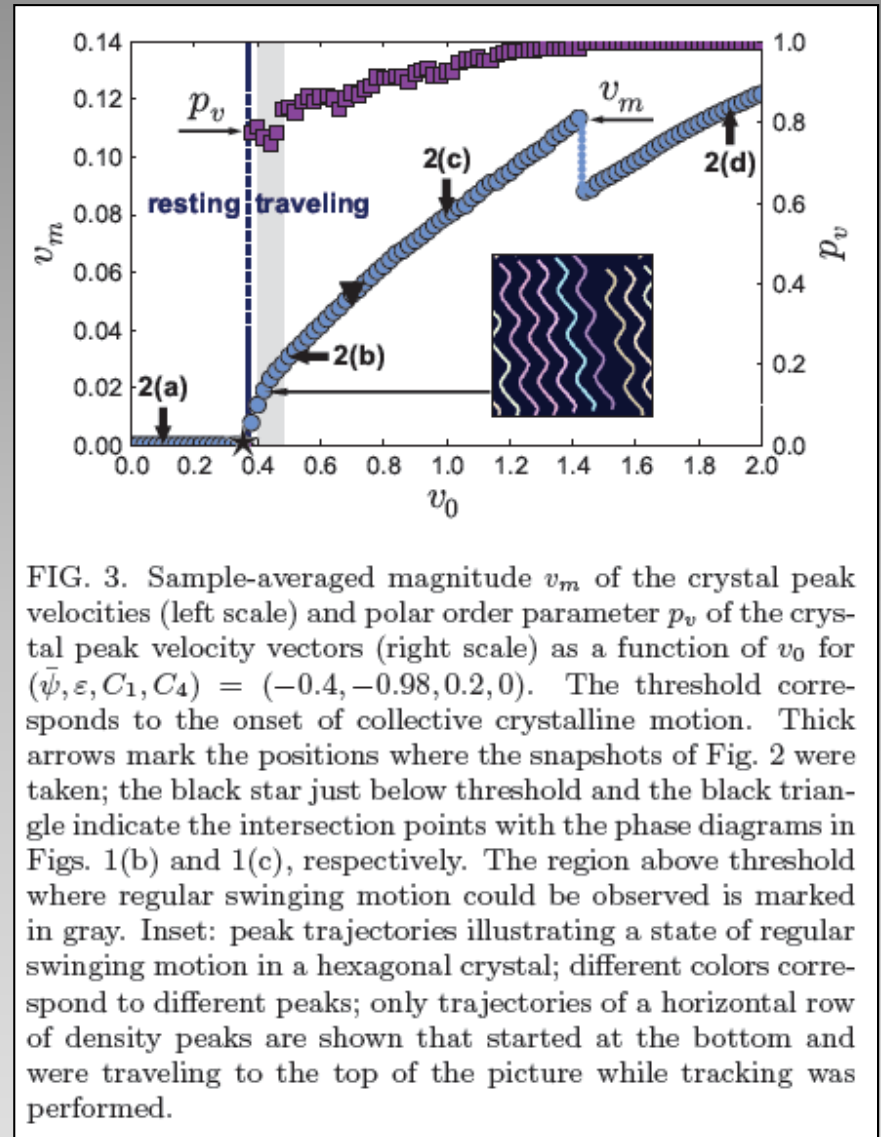
FIG. 3. Sample-averaged magnitude v_m of the crystal peak velocities (left scale) and polar order parameter p_v of the crystal peak velocity vectors (right scale) as a function of v_0 for $(\bar{\psi}, \varepsilon, C_1, C_4) = (-0.4, -0.98, 0.2, 0)$. The threshold corresponds to the onset of collective crystalline motion. Thick arrows mark the positions where the snapshots of Fig. 2 were taken; the black star just below threshold and the black triangle indicate the intersection points with the phase diagrams in Figs. 1(b) and 1(c), respectively. The region above threshold where regular swinging motion could be observed is marked in gray. Inset: peak trajectories illustrating a state of regular swinging motion in a hexagonal crystal; different colors correspond to different peaks; only trajectories of a horizontal row of density peaks are shown that started at the bottom and were traveling to the top of the picture while tracking was performed.

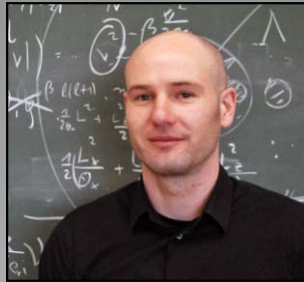A. M. Menzel, HL, PRL **110**, 055702 (2013)

V) Phase separation for active particles

Julian Bialké

Thomas Speck

motility-induced phase separation

(Tailleur and Cates)

spherical particles (one segment)

rotational noise decoupled (minimal model)

interaction coupling parameter $\quad \Gamma = v_0 \sqrt{\rho} \big/ k_B T$

propulsion strength

$$p_e = \frac{F}{k_B T \sqrt{\rho}}$$

I. Buttinoni, J. Bialke, F. Kümmel, H. Löwen, C. Bechinger, and T. Speck, PRL **110**, 238301 (2013)

See also: J. Palacci, S. Sacanna, A. P. Steinberg, D. J. Pine, and P. M. Chaikin, Science **339**, 936 (2013);   G. Gregoire, H. Chate, Y. Tu, Physica D **181**, 157 (2003)
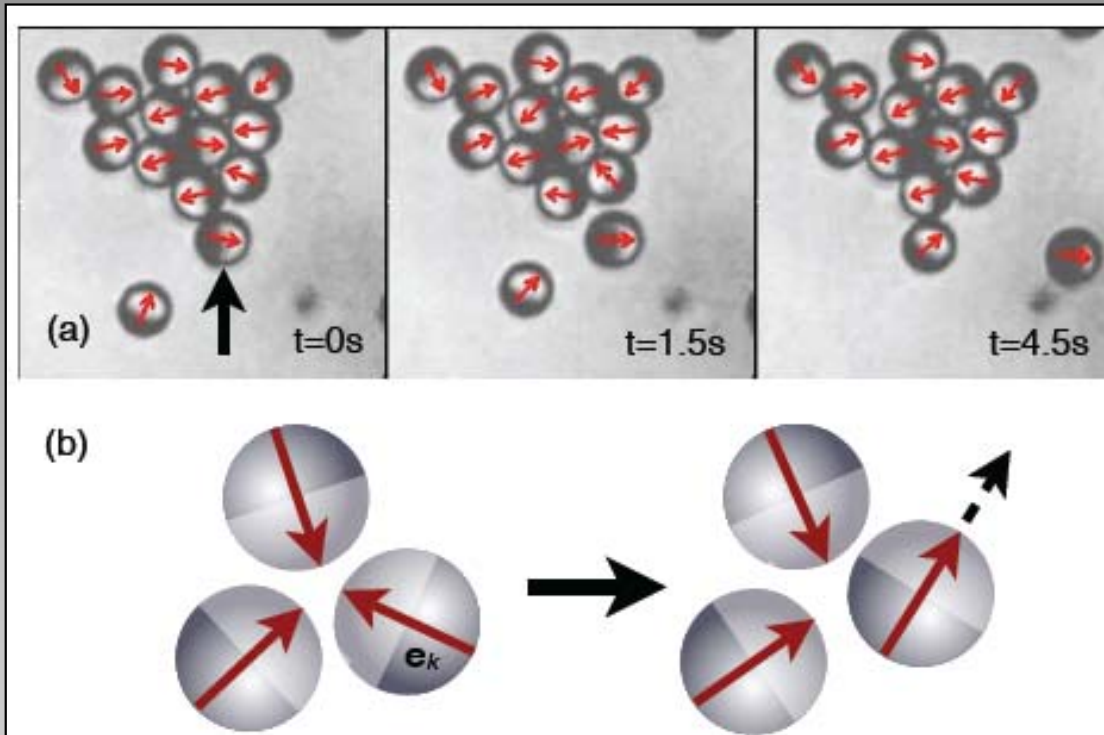
the mechanism of clustering

FIG. 5: (a) Consecutive close-ups of a cluster, where we re-solve the orientations (arrows) of the caps. Particles along the rim mostly point inwards. The snapshots show how the indicated particle towards the bottom (left) leaves the cluster (center) and is replaced by another particle (right). (b) Sketch of the self-trapping mechanism: for colliding particles to become free, they have to wait for their orientations to change due to rotational diffusion and to point outwards.

simulation

Pe = 40

Pe = 80

experiment

I. Buttinoni, J. Bialke, F. Kümmel, H. Löwen, C. Bechinger, and T. Speck, PRL **110**, 238301 (2013)
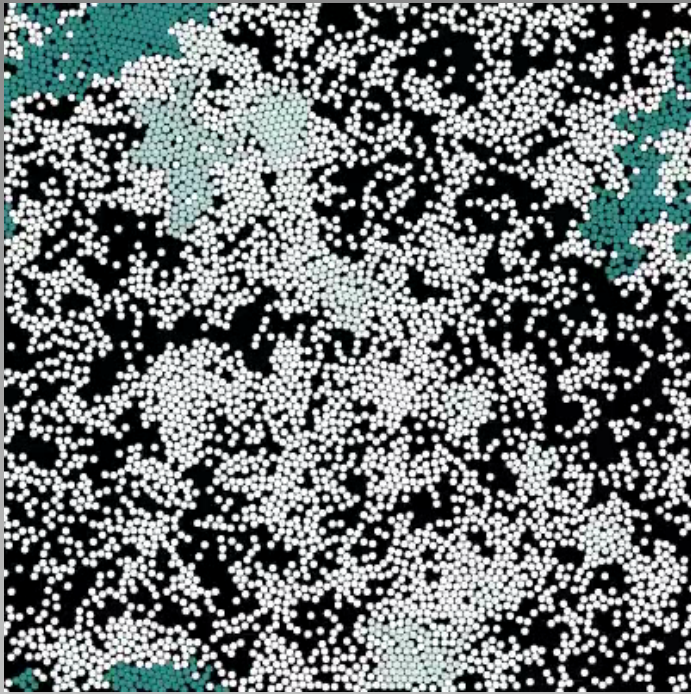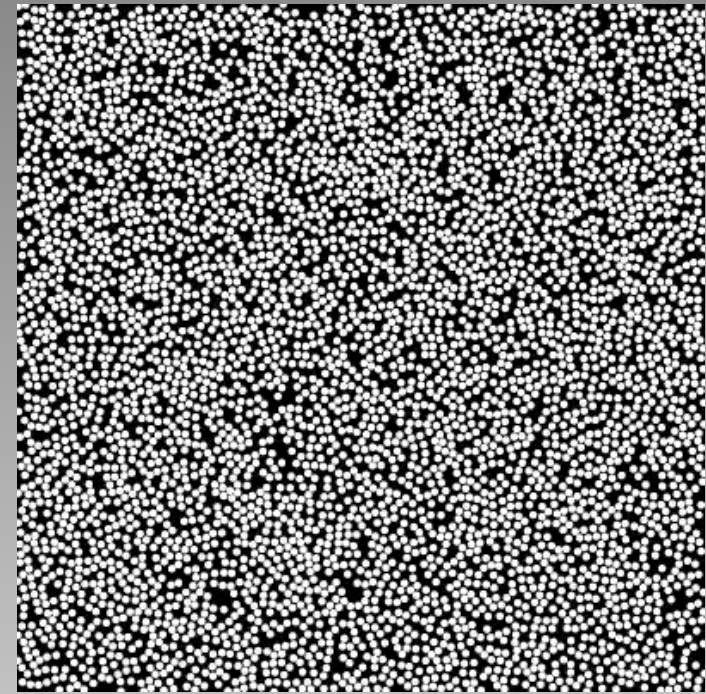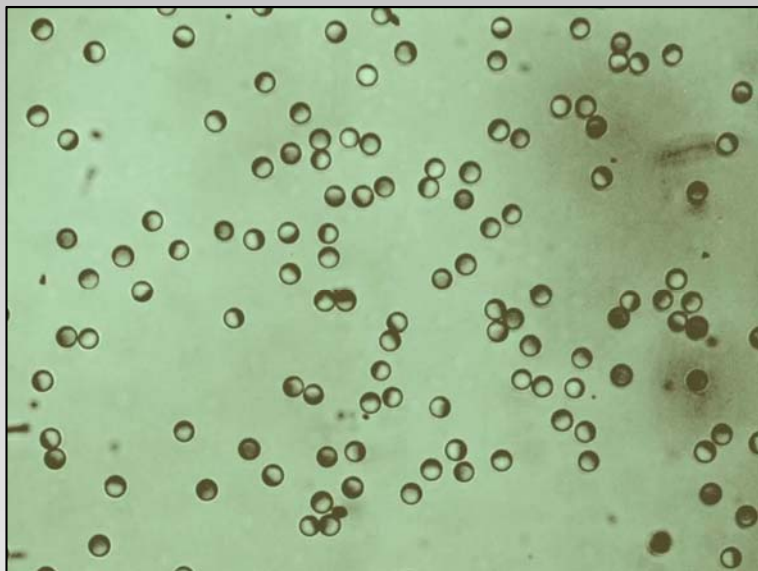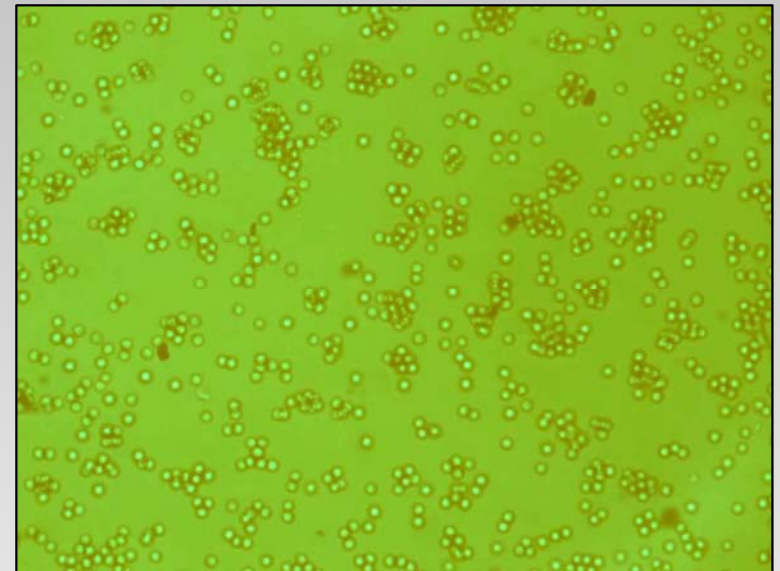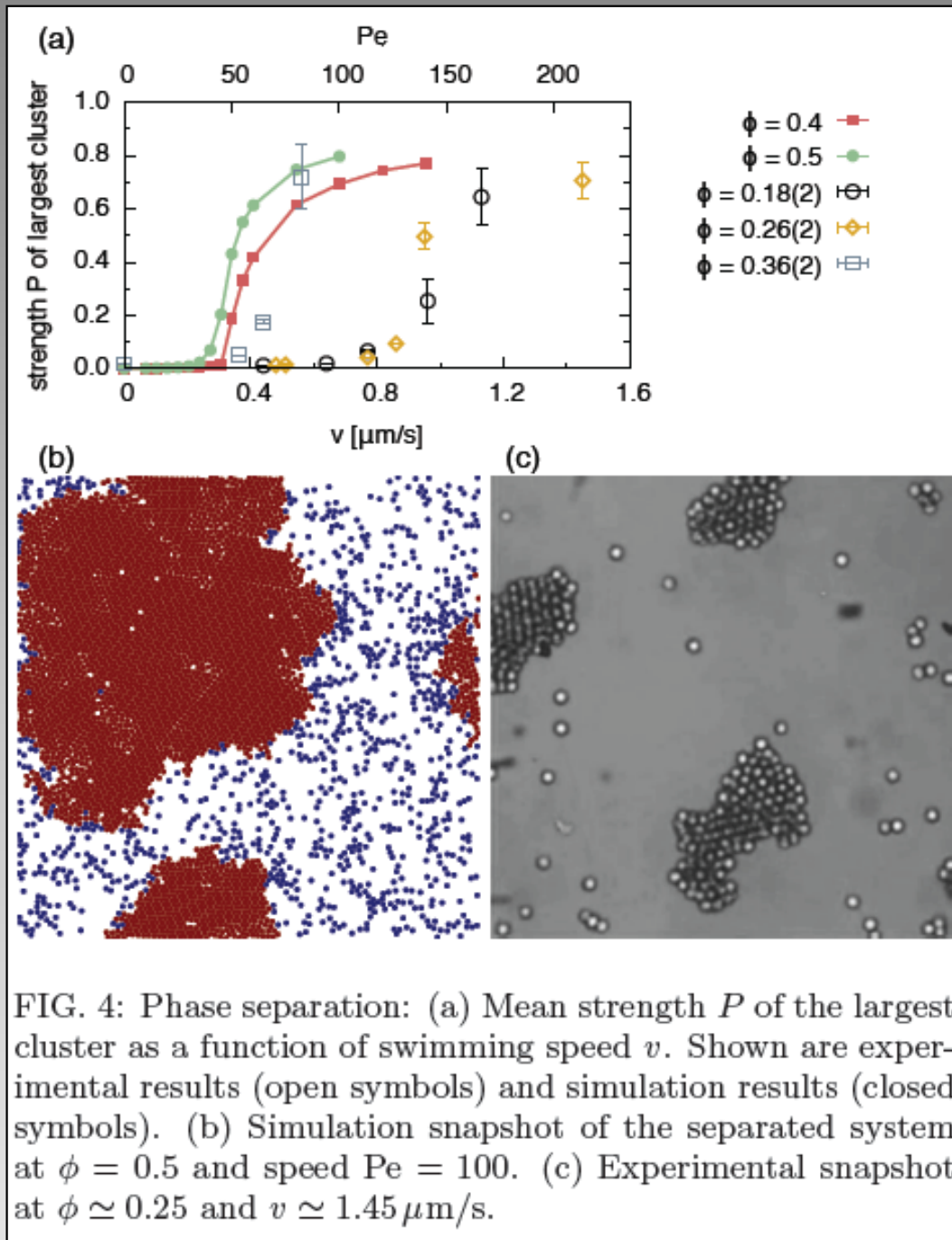
FIG. 4: Phase separation: (a) Mean strength P of the largest cluster as a function of swimming speed v. Shown are experimental results (open symbols) and simulation results (closed symbols). (b) Simulation snapshot of the separated system at $\phi = 0.5$ and speed Pe $= 100$. (c) Experimental snapshot at $\phi \simeq 0.25$ and $v \simeq 1.45\,\mu\text{m/s}$.

I. Buttinoni, J. Bialke, F. Kümmel, H. Löwen, C. Bechinger, and T. Speck, PRL **110**, 238301 (2013)

instability theory

Fig. 3. Simulation results neglecting translational diffusion for: (H) soft spheres with harmonic repulsion, (GCM) the Gaussian core model, and (Y) the Yukawa potential.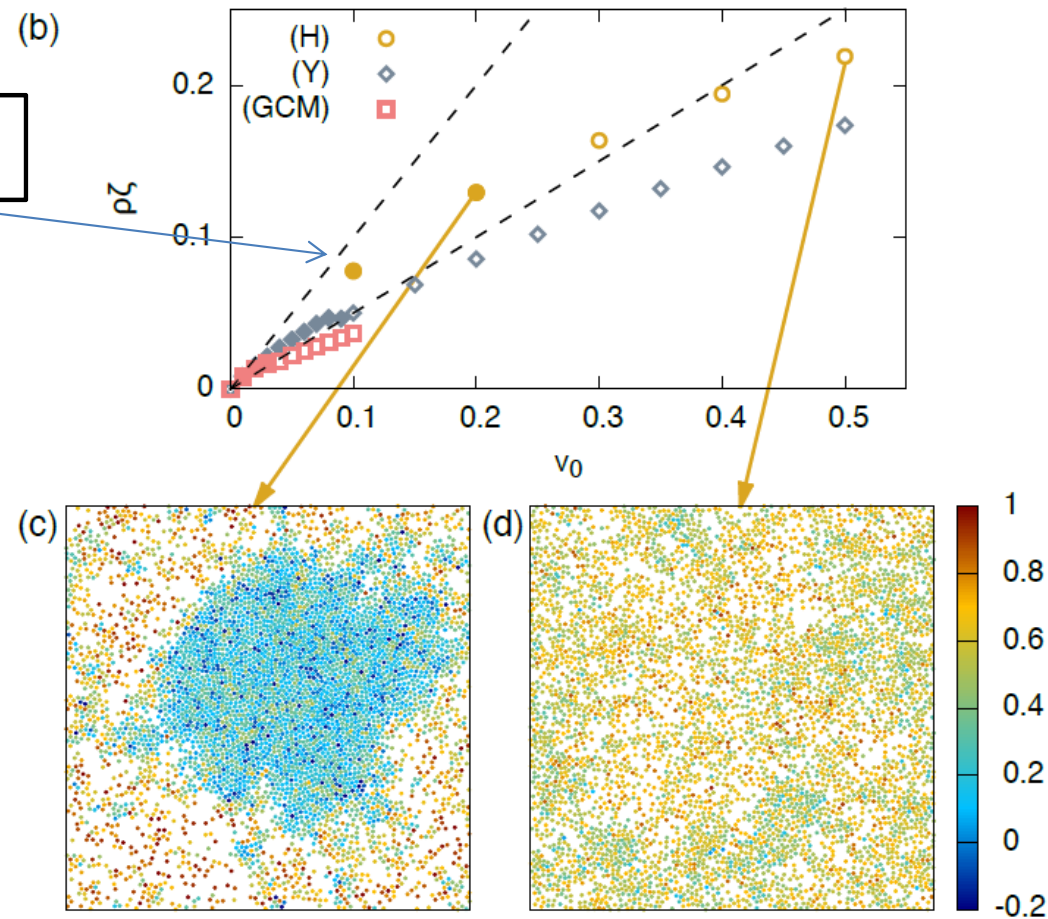 (a) Structure factors $S(q)$ for different speeds v_0 increasing from bottom to top. (b) Force coefficient ζ as a function of the propulsion speed v_0 (note that the unit of time compared to Fig. 2 is $1/100$). Open symbols correspond to homogeneous systems, closed symbols to phase separated systems. (c) Snapshot at speed $v_0 = 0.2$ and (d) at speed $v_0 = 0.5$ for (H). Every particle is colored according to Eq. $[27]$ with $\Delta t = 25$ quantifying the persistence of particle motion with respect to the initial particle orientation.

For more details: J.Bialké, T.Speck, H.Löwen, EPL **103**, 30008 (2013)

scaling of cluster growth for coagulating particles

(a) $\beta = 1 + \gamma$

(b) $\beta = \frac{d-1}{d} + \gamma$

(c) $\beta = \frac{1}{2} + \gamma$

(d) $\beta = \frac{d-1}{2d} + \gamma$

Fig. 1: Four cases for the scaling exponent β of the total propulsion force F_N with cluster size N in d spatial dimensions. The arrows denote the directions of single particle contribution forces.
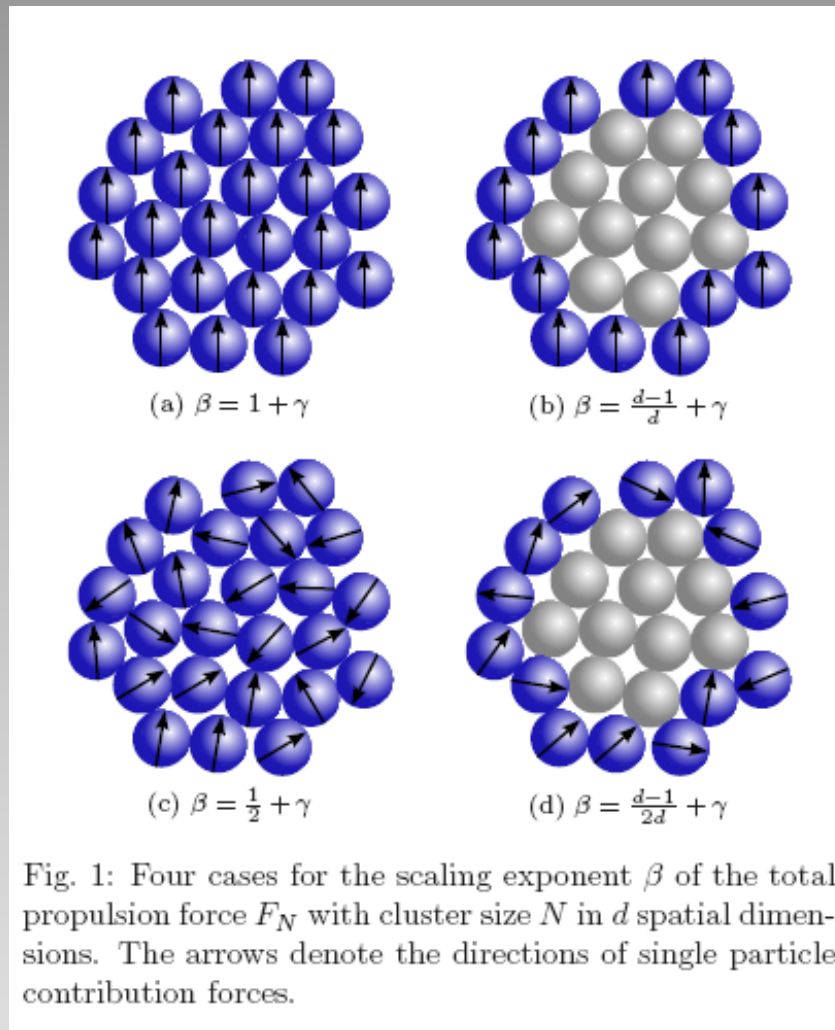
$$N_C \propto t^{\gamma}$$

explosive growth possible $N_C \to \infty$ for $t \to t_0 < \infty$

P. Cremer, H. Löwen, Phys. Rev E **89**, 022307 (2014)

Simple „sweeping argument" to derive scaling (in the ballistic regime)
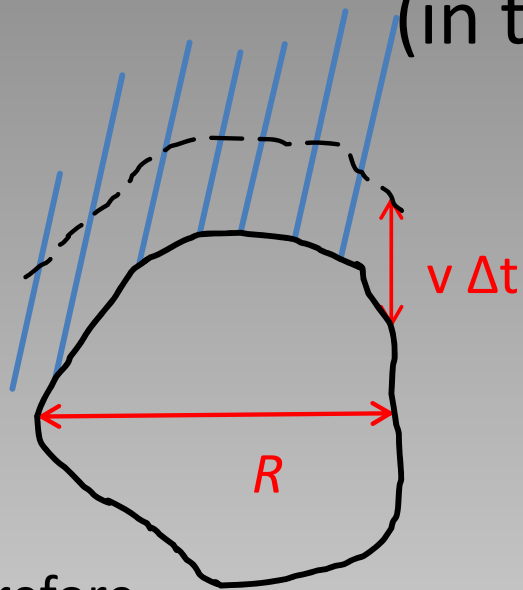
number density ρ of particles

$$R \propto N_C^{\frac{1}{d}}$$

in time interval Δt the cluster sweeps out a volume of $v \, \Delta t \, R^{d-1}$

v Δt

R

Therefore

$$\Delta N_C = \rho \, R^{d-1} \, v \, \Delta t \qquad v \propto N_C^{\beta - \frac{1}{d}}$$

$$\Rightarrow \dot{N}_C \propto N_C^{\beta + (d-2)/2}$$

$$N(t) = \begin{cases} \left[N_0^{2/d-\beta} + C(2/d - \beta)t \right]^{\frac{1}{2/d-\beta}} & \beta < 2/d, \\ N_0 \exp(Ct) & \beta = 2/d, \\ C(\beta - 2/d)\,(t_c - t)^{\frac{-1}{\beta - 2/d}} & \beta > 2/d, \end{cases}$$

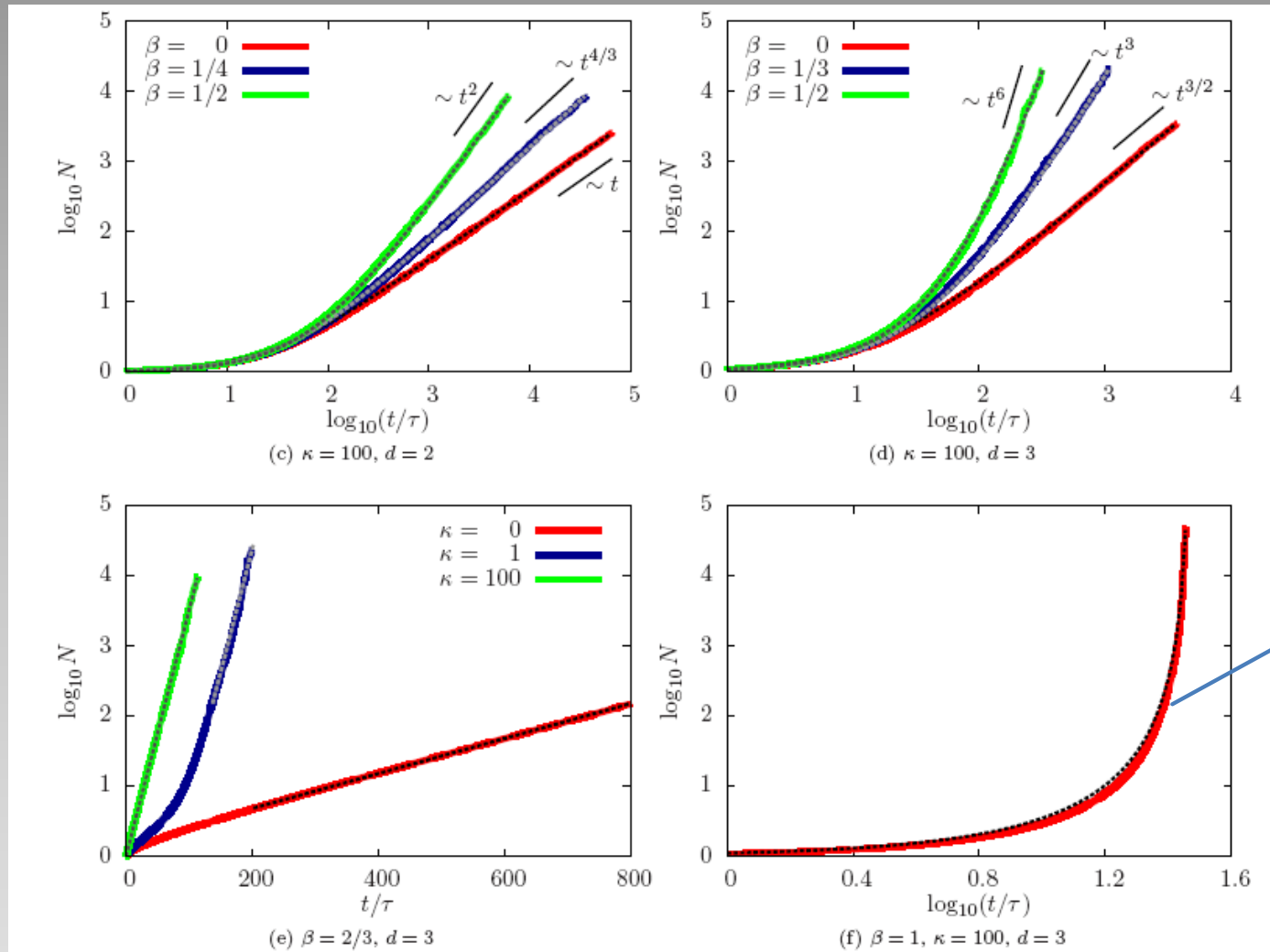# Confirmation of the scaling predictions by particle resolved simulations

Fig. 3: Cluster size evolution obtained from simulations in $d = 2, 3$ dimensions with various values of the persistence parameter κ and the total propulsion force scaling exponent β. Algebraic growth in the diffusive regime (a), (b) as well as in the ballistic regime (c), (d) occurs with the predicted exponents as indicated in the plots. Exponential growth (e) in the ballistic regime occurs faster than in the diffusive regime as indicated by the much higher slope. For high persistence and high force scaling, explosive cluster growth occurs (f). The dashed lines are fits using eqs. (3) and (4) respectively.

Summary

- Active particles exhibit phase separation purely induced by the drive

- New scaling behaviour

- Nucleation?

VI) Conclusions

active colloidal particles reveal
fascinating collective features!

Thanks to:

U. Zimmermann, B. ten Hagen, R. Wittkowski, C. Hoell, A. Menzel, J. Bialké,
T. Speck, A. Kaiser, K. Popowa, P. Cremer, S. Babel

Collaboration with: H. H. Wensink (Paris), J. Dunkel (MIT), R. Goldstein,
K. Drescher (Cambridge), J. Yeomans (Oxford), S. van Teeffelen (Princeton),
S. Heidenreich (Berlin), I. Aranson (Argonne),
C. Bechinger (Stuttgart), T. Palberg (Mainz)